



New approaches to dating intermittently varved sediment, Columbine lake, Colorado, USA

Stephanie H. Arcusa¹, Nicholas P. McKay¹, Charlotte Wiman², Sela Patterson¹, Samuel E. Munoz^{2,3}, Marco A. Aquino-López⁴

5 ¹School of Earth and Sustainability, Northern Arizona University, Flagstaff, 86011, USA

²Department of Marine and Environmental Sciences, Northeastern University, Marine Science Center, Nahant, 01908, USA

³Department of Civil and Environmental Engineering, Northeastern University, Boston, 02115, USA

⁴Centro de Investigación en Matemáticas (CIMAT), Jalisco s/n, Valenciana, 36023 Guanajuato, Gto, Mexico

Correspondence to: Stephanie H. Arcusa (sha59@nau.edu)

10 **Abstract.** Annually laminated lake sediment can track paleoenvironmental change at high-resolution where alternative archives are often not available. However, information about both paleoenvironmental change and chronology are often affected by indistinct and intermittent varves. We present an approach that overcomes these and other obstacles by using a quantitative varve quality index combined with a multi-core, multi-observer Bayesian varve sedimentation model that quantifies realistic under- and over-counting uncertainties while integrating information from radiometric measurements
15 (²¹⁰Pb, ¹³⁷Cs, and ¹⁴C) into the chronology. We demonstrate this approach on thin sections of indistinct and intermittently varved sequences from alpine Columbine Lake, Colorado. The integrated model indicates 3137 (95 percentile highest density probability range: 2753-3375) varve years with a cumulative posterior distribution of counting uncertainties of -13/+7 % indicative of systematic observer undercounting. The sedimentary features of the thin and complex varves shift through time, from normally graded couplets to couplets interrupted with coarser sub-laminae, to inversely graded couplets.
20 We interpret the normal grading couplets as spring nival discharge followed by winter settling, the coarser sub-laminae as high rainfall events, and the inverse grading as hyperpycnal flows and/or pulses of dust related to human impact changing the varve formation mechanism. Our novel approach provides a realistic constraint on sedimentation rates and quantifies uncertainty in varve counts by quantifying over- and under-counting uncertainties related to observer bias and the quality and variability of the sediment appearance. The approach permits the construction of a varve chronology and sedimentation
25 rates for sites with intermittent or indistinct varves, which are likely more prevalent than sequences with distinct varves, and thus, expands the possibilities of reconstructing past environmental change with high resolution.

1 Introduction

The establishment of a reliable chronology for lake sediment is a pre-requisite of paleoenvironmental investigation. As many studies have pointed out, low age uncertainty is necessary to compare events through space, time, and archive (Zimmerman
30 and Wahl, 2020). To that end, annually laminated sediment (i.e., varves) not only presents a unique opportunity to



reconstruct variability on a seasonal to annual scale, it allows for the quantification of sediment accumulation rates on shorter timescales than sequences dated by radiometric techniques (Boers et al., 2017). Sedimentation rates are useful for a wide range of investigations, but especially so for the accurate calculation of fluxes ($\text{g cm}^{-2} \text{yr}^{-1}$) of sedimentary constituents. For paleoenvironmental reconstructions, flux is typically a more meaningful measure than abundance or concentration
35 because it considers changes in the sediment due to time and density. For example, investigations using lake sediment of past aerosol deposition such as dust report different conclusions when flux is used compared to abundance (Arcusa et al., 2019; Routson et al., 2016, 2019). The importance of constraining age and sedimentation rate uncertainty is increasingly recognized and the tools to handle this uncertainty are constantly improving (Aquino-López et al., 2018; McKay et al., 2020).

40

Despite general improvements, the quantification of uncertainty in varved sediments remains focused on counting. Although there is no standard method for calculating uncertainties in varve chronologies, most are associated with $\pm 1-4\%$ counting uncertainty with some indistinctly varved sequences having counting errors up to $\pm 15\%$ (Ojala et al., 2012). Counting errors are often quantified as the root mean squared error of counts from multiple observers along defined transects on multiple
45 cross-dated cores from the same site either as maximum and minimum deviations from the mean or as replicated counts between marker layers (Lamoureaux, 2001). Reported error estimates commonly do not include all known error sources.

Error sources are associated with (1) inter-site differences in varve counts (missing varves), (2) subjectivity in identifying varves due to varve quality, (3) expert judgement in identifying marker layers, (4) compound single varves that are mis-
50 interpreted as representing multiple years (over counting), (5) indistinct varves that are combined with adjacent varves (under counting), (6) intermittent (floating) varves, (7) technical issues (missing varves), and (8) counting strategies (Fortin et al., 2019; Ojala et al., 2012; Żarczyński et al., 2018; Zolitschka et al., 2015). Although these various sources are often considered individually, they are less frequently considered in concert and rarely considered when estimating sedimentation rates. The variety of error sources makes their quantification an important challenge, especially for sequences with indistinct
55 or intermittent varves.

Sedimentary sequences with indistinct or intermittent varves cannot be used to develop a chronology with conventional techniques as the massive sediment or indistinct laminations result in information loss. The problem is often addressed by subjectively applying the sedimentation rate estimated from neighboring varved sections, although more mechanistic
60 methods have also been developed. For example, Schlolaut et al. (2012) describe a procedure that analyses the seasonal layer distributions to estimate the number of years of sediment accumulation represented. Although promising, such a method of varve interpolation has yet to be integrated with a complete accounting of all other errors.



65 Few previous works have attempted to assess errors associated with varve counts by their sources. For example, Fortin et al. (2019) developed a Bayesian probabilistic model to incorporate three sources of uncertainty related to the subjectivity in identifying varves, inter-site differences, and a combination of the likelihood of over- and under-counting by the observer and the proper identification of isochronous marker layers. Although this model provided a clearer picture of the sources of uncertainty, it did not go as far as addressing the problem of indistinct varves (such as those deposited during the 20th century as glacier influence waned) nor quantifying the impact of varve quality on the chronology.

70

Additionally, errors can be systematic in that the net outcome is one of over- or under-counting. These systematic biases are typically assessed by comparing the varve chronology to radiometric methods (^{137}Cs , ^{210}Pb , and ^{14}C) and can sometimes be corrected. For example, the agreement between varve and radiometric chronologies can be evaluated objectively through OxCal's V_sequence, for example (Bronk Ramsey, 1995; Tian et al., 2005; Zander et al., 2019). The ^{14}C ages can reveal 75 missing sediment intervals where missing varves can be inserted (Tian et al., 2005). However, the process has two major drawbacks. First, the ^{14}C ages could be too old, or, if they are correct, the location of the nonconformity in the sedimentary sequence might be misplaced. Second, this approach does not constrain the uncertainty introduced into the estimation of the sedimentation rate.

80 Here, we present an approach to quantify age and sedimentation rate uncertainty using multiple cores and observers as demonstrated in a case study of an indistinctly and intermittently varved sequence from Columbine Lake, Colorado. We expand on the Fortin et al. (2019) Bayesian model to include uncertainty from multiple observers, varve interpolation, and varve quality. We then use Bayesian learning to update prior estimates of the counting uncertainties given the constraints from independent radiometric ages. Partly because continuous chronologies are rare, no late Holocene varve sequence has 85 been published from the southern Rocky Mountains up to now. Moreover, the nearest published varved lake record is 250 km away (Anderson et al., 2010). The chronology developed here provides the foundation for future high-resolution paleoenvironmental research at Columbine Lake.

2 Study Site

90 Columbine Lake (37.8622° N, 107.7717° W, elevation 3874 m) is a deep, mildly acidic (pH 5), oligotrophic lake in San Juan County, Colorado (Fig. 1). The lake bathymetry is marked by deep pockets, with a maximum depth of 27 m. Deep and small sub-basins favor seasonal stratification and anoxic conditions necessary for varve formation (Zolitschka et al., 2015). The lake is fed by a small pond and stream to the northwest and drained by Mill Creek to the northeast. The catchment bedrock is andesite emplaced during the late and middle Tertiary (Lipman and McIntosh, 2011), and less than 5 % of the area was vegetated in 2017 (Arcusa et al., 2019). The catchment is currently unglaciated and shows no evidence for rock glaciers. The



95 closest documented evidence of a Little Ice Age moraine is near Trinity Peaks (Carrara, 2011). There are no access roads, but historic mining activity is evident at lower elevations and the lake outflow is raised by a 2-m-high earthen dam.

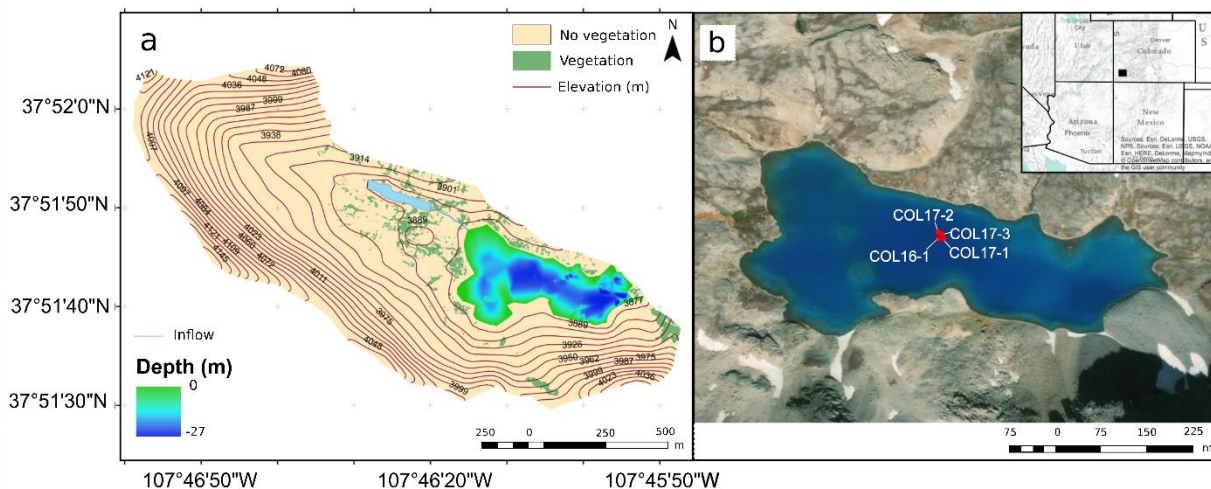


Figure 1. Columbine and its catchment showing (a) bathymetry and (b) coring location (red circles) in southwest Colorado (black rectangle in inset map). Vegetation extent for the year 2017 based on Arcusa et al. (2019). Image credit: Esri, DigitalGlobe, GeoEye, Earthstar Geographics, CNES/Airbus DS, USDA, USGS, AeroGRID, IGN, and the GIS User Community.

100

The climate of Silverton, Colorado (elevation 2865 m) near the study site is typified by a biseasonal climate. Over 80 % of precipitation falls predominantly as snow from October to March (average 560 mm/month total snowfall) from Pacific frontal storms, and summer rainfall is associated with the northern extent of the North American Monsoon (Jul-Sep, average 70 mm/month). Average winter (DJF) and summer (JJA) temperature ranges are -18.8 to 2.5 °C and -0.1 to 22.8 °C, respectively (Western Regional Climate Center, 2018). Like much of the Southwest United States, the El Niño Southern Oscillation (ENSO) teleconnection usually results in wet winters during El Niño and dry winters during La Niña (Sheppard et al., 2002).

105

110 3 Methods

3.1 Coring

Four sediment cores were collected from Columbine Lake at water depths ranging from 25 to 27 m. One 81-cm-long core was taken in August 2016 (COL16-1) using an aquatic corer, and three 125- to 142-cm-long cores were collected in September 2017 (COL17-1, COL17-2, and COL17-3) using a modified UWITECH percussion coring system. All three 2017

115



the Sedimentary Records of Environmental Change Lab at Northern Arizona University. Consistent core stratigraphy and marker layers found in all cores except COL17-1 facilitated visual core cross-correlation (**Error! Reference source not found.** Fig. A1). Core COL17-1 is not laminated, possibly because it was collected at shallower depth, and was not considered further in this study.

120 3.2 Non-destructive core analysis

To support the visual correlations, cores COL16-1, COL17-2, and COL17-3 were analyzed for non-destructive methods. First, magnetic susceptibility (MS) was measured at 1 cm increment (2 cm measurement diameter resolution) using a Bartington MS2 surface sensor. Then, X-Ray Fluorescence (XRF) was measured at 0.5 and 1 cm intervals (1 cm measurement diameter resolution) at 10, 30, and 50 kV using an Avaatech core scanner at Texas A&M University, College
125 Station. Finally, hyperspectral imaging in the visible to near-infrared range was measured at ~68 $\mu\text{m}/\text{pixel}$ using a Specim Ltd. core scanner equipped with a PFE-xx-V10E camera at Northern Arizona University following the method by Butz et al. (2016). The hyperspectral data were used to calculate indices shown to be related to chlorophyll and its degradation products (RABD660) (Trachsel et al., 2010; Yackulic, 2017) as well as chlorite (minimum peak) (Rein and Sirocko, 2002).

3.3 Destructive core analysis

130 To support the sedimentological facies interpretation, various destructive analytical analyses were performed on core COL17-3. Loss-on-ignition and wet and dry bulk density following Dean (1974) used 1-2 cm^3 of sediment weighed wet and dry after freeze-drying for 12 hours, then weighed after burning at 550 $^{\circ}\text{C}$ for 5 hours in the furnace. An aliquot of 80 mg of material was then used for quantifying the abundance of biogenic silica following an adapted procedure of Mortlock and Froelich (1989). Briefly, the samples were pre-treated to remove organics. Biogenic silica was brought to a solution and
135 measured by spectrophotometry. Finally, an aliquot of 200 mg of material was used for grain size analysis. The initial procedure was the same, but the solution of biogenic silica was discarded. Then, sodium hexametaphosphate was added as a dispersant and shaken for 3 hours. Grain size distributions in the 0.04–2000 μm range with 116 classes were analyzed using a laser diffraction Coulter LS13-320 and each sample was measured 5 times.

3.4 Geochronology

140 This study added three radiocarbon dates to the three previously published by Arcusa et al. (2019) on cores COL17-3 and COL16-1. Macrofossil of terrestrial plants and aquatic insects were pre-treated using standard acid–base–acid procedures and analyzed for radiocarbon activity on Northern Arizona University's MICADAS equipped with the Gas Interface System while it was located at the manufacture's (IonPlus) office in Zurich, Switzerland. In addition to radiocarbon, Arcusa et al. (2019) also measured ^{210}Pb and ^{137}Cs activities respectively on 20 and 16 dried and homogenized samples over the top 12.5
145 cm of core COL17-3 using a Canberra Broad Energy Germanium Detector (BEGe; model no. BE3830 P-DET) at the Marine Science Center at Northeastern University.



The radiometric age-depth model was constructed from the concurrent use of Bayesian modeling R software packages Bacon (Blaauw and Christen, 2011) and Plum (Aquino-López et al., 2018). Briefly, Plum is based on a statistical framework, which uses statistical inference to provide more robust and realistic uncertainties when compared to the Constant Rate of Supply (CRS) method (Appleby and Oldfield, 1978). The concurrent use of Bacon and Plum reduces the artificial break in sedimentation rates at the intersection of the ^{210}Pb and ^{14}C ages, and Plum provides a more natural merger of these techniques as it does not require the pre-modeling of the ^{210}Pb dates. Additionally, we compare Plum to conventional calculations of CRS (Appleby, 2001) and the Constant Flux Constant Sedimentation (CFCS) method (Krishnaswamy et al., 1971) implemented with the R package SERAC (Bruel and Sabatier, 2020).

3.5 Thin sections, sediment imaging, and point measurements

To facilitate investigation, measurement, and counting of the fine laminations, the sediment was subsampled and impregnated with low viscosity epoxy resin following a modified approach of Lamoureux (1994). The percentage of epoxy to acetone was increased multiple times before fully embedding the sediment. Overlapping sediment slabs (7.0 x 3.0 x 1.5 cm) were sampled and placed in an acetone bath for fluid replacement. Acetone was exchanged every 12 hours for five days until no water was left in the sediment. Following fluid displacement, Spurr's Low Viscosity Embedding Resin was exchanged every 12 hours for three days and left to cure for one day at room temperature followed by one day at 40 °C, one day at 50 °C, and one day at 60 °C. Slabs were cut at the Northern Arizona University machine shop and sections were sent to Quality Thin Sections in Tucson, AZ, for mounting and polishing. Images of the thin sections were taken at 2x and 10x magnification under polarized light with a calibrated petrographic polarizing microscope (Carl Zeiss Axiophot) connected to a digital camera (Carl Zeiss AxioCam) and automated stepping stage (PETROG System, Conwy Valley Systems Ltd (CVS), UK). Individual images were stitched into a mosaic using the Stitching plugin (Preibisch et al., 2009) in ImageJ.

To categorize and interpret varve facies, microscopic analyses of elemental composition and grain size are sometimes used (Cuven et al., 2010; Żarczyński et al., 2019a). In this study, the varves were thinner than the sampling resolution of either destructive (BSi and grain size) or non-destructive (XRF, hyperspectral, and MS) procedures available. Therefore, we used point counts and length measurements directly on individual grains in the slides. At least 100 grains were measured from the varve transects.

3.6 Statistical analyses

To support the interpretation of the sedimentary facies, statistical analyses were performed on the results from both destructive and non-destructive procedures. First, the values were binned to match the sampling resolution of the dataset with the lowest resolution using the function bin2d in the R package geoChronR (McKay et al., 2021). Second, the values were standardized to a mean of zero and variance of one standard deviation. Then to identify distinct stratigraphic units,



180 hierarchical cluster analysis was applied using the function `chclust` R package `rioja` (Juggins, 2020). To associate units to the variables explaining the most variance, a principal component analysis that was applied with the function `PCA` in the R package `FactoMineR` (Lê et al., 2008). Finally, to explore the relationship between variables, correlation analysis was performed using Spearman's rank as the data distribution failed the Shapiro-Wilks normality test in most cases ($p < 0.05$).

3.7 Varve chronology

3.7.1 Description of the original varve model

185 The data analysis in this study expands on the original R (R Core Team, 2019) package `varveR` (McKay, 2019) that builds varve chronologies while quantifying uncertainty as it relates to varve identification, inter-site differences, and likelihoods of over- and under-counting. `varveR` is a Bayesian probabilistic model that quantifies age uncertainty by integrating information from the age distribution of marker layers from multiple cores (Fortin et al., 2019). The model follows two concepts. First, it uses the sedimentological understanding of the likelihood of the correct delineation of the varves such as those related to the ease of distinguishing them. Second, it takes advantage of the replication from the marker layers correlating between cores to quantify the likelihood of under- and over-counting and the uncertainty in the total count as a function of depth.

195 The model's inputs include (1) thicknesses for each varve for each core, (2) site-specific marker layers to stitch the thin sections together into a varved sequence, and (3) inter-site marker layers. In this study, thickness delineations were created as ArcMap shapefiles. Site-specific marker layers were identified in the overlap between two adjacent thin sections. Inter-site marker layers were identified in each core for cross-correlation. All three were identified by three observers working independently to explore uncertainties associated with expert judgment.

200 The model uses prior likelihoods of over- and under-counting and updates them as it iterates. The prior likelihoods are selected by the operator but may be the difference in the number of varves counted by two observers expressed as a percentage and converted into a probability, for example (Fortin et al., 2019). With each iteration, the only constraint is that the duration across cores between marker layers must be the same. `varveR` outputs an n -member ensemble of varve counts and thicknesses for each core and a composite of all cores, where n is a user-defined number of iterations. The ensemble is used to quantify the uncertainty in depth as a function of varve year and can be transposed to estimate uncertainty in varve year as a function of depth. The model is completely independent from radiometric age control.

3.7.2 Modifications to the original model: varve quality index and varve emulator

We expanded the `varveR` model to include information on varve quality as an indicator of the likelihood of over- and under-counting. Although varve quality indices have been used in past research as a qualitative aide to interpretation (Bonk et al.,



210 2015; Dräger et al., 2017; Żarczyński et al., 2018), here we integrate this information quantitatively. Each varve was associated with a code (1, 2, or 3) (Appendix A Fig. A2) with a corresponding distribution of over and undercounting prior probability estimate (Sect. 3.7.3). The codes are assigned by the clarity of the varve's appearance, with a code value of 1 being of higher clarity than a code value of 3. A code of 4 was used when it was difficult to distinguish whether two couple represented one or two years. In this case, they were counted as two varves, and denoted with a code of 4, which were
215 assigned a 50 % probability of over-counting. The application of code 5 is described below. Finally, sections where sediment is likely missing for technical reasons (e.g., between two adjacent thin sections without overlap or in gaps created during the embedding process), were assigned a code of 6, and varves were similarly emulated although the number of missing years is unknown.

220 Distinctly varved sediments are interspersed with indistinctly varved sections, which comprise zones up to 2 cm thick with weakly defined to no visible laminations (Appendix A Fig. A2). These indistinct sections were relatively common, comprising 8.7-19.6 % of the total sediment thickness across observers. For these sections, a code of 5 was assigned. Previous studies have addressed the issue of indistinct varve sections by either interpolating sedimentation rates from nearby varved segments (e.g. Hughen et al., 2004), or using the probability distribution of the varves' seasonal layers to derive
225 sedimentation rates (Schlolut et al., 2012). Because our varveR approach requires an estimate of varve thicknesses for each year rather than an estimate of mean sedimentation rate or missing time, these solutions are insufficient. Instead, we simulate varves through these sections.

To simulate varves in indistinct intervals, we developed a varve emulator that randomly chooses a distinctly varved section
230 of the core and with a length of that section matches the thickness of the interval as nearly as possible. Because laminations at Columbine Lake are very thin (typically < 0.5 mm) relative to the thickness of the indistinct intervals (typically ~ 4 mm), this procedure alone matches the cumulative depth closely. Subsequently, a minute thickness adjustment is applied across the sequence to ensure a perfect match in total thickness and conservation of the depth of the core. This approach is reasonable where other varved intervals can serve as reasonable surrogates for indistinct sections. We argue this is the case for
235 Columbine Lake, as the distribution of the varve thickness is similar in both cores throughout the sections with distinct varves (Appendix A Fig. A3). Furthermore, there is no evidence for systematic changes in the mode of deposition in these sections, as the indistinct sections occur throughout both cores, but not always at the same time and the sedimentary features were mostly the same above and below the indistinct sections.

3.7.3 Chronology with symmetrical and asymmetrical uncertainty

240 The modified varveR model was used to build two varve chronologies each following a different scenario. In both scenarios, codes 1, 2, and 3 were given over- and under-counting priors. In the first scenario, the priors were symmetrical and based on values found in the literature (Fig. 2a; e.g. Dräger et al., 2017). This was done to produce a chronology that would resemble



the conventional varve chronology construction and allow for comparison. However, due to missing or indistinct varves, varve chronologies are often subject to under-counting (Tian et al., 2005; Żarczyński et al., 2018). Because the varves in this lake are thin and often lacked clarity in their appearance, we considered a symmetrical prior to be unrealistic for Columbine Lake. A prior shifted towards under-counting was deemed more representative. Therefore, in a second scenario, we assigned wider symmetrical priors for code 1, wider asymmetrical priors for code 2, and assigned an uninformed asymmetrical prior for code 3 (Fig. 2b). This expanded version of varveR incorporates uncertainty pertinent to varve quality, inter-site variation, expert judgment (Fig. 3).

250

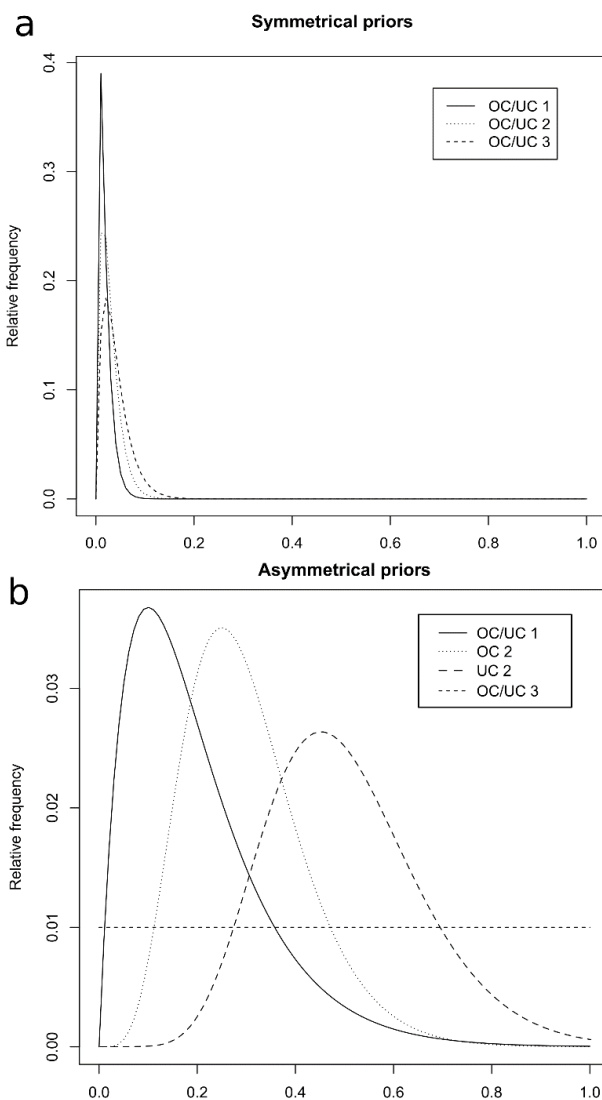




Figure 2. Varve quality codes and their associated under- (UC) and over-counting (OC) gamma distribution priors for (a) symmetrical and (b) asymmetrical varveR.

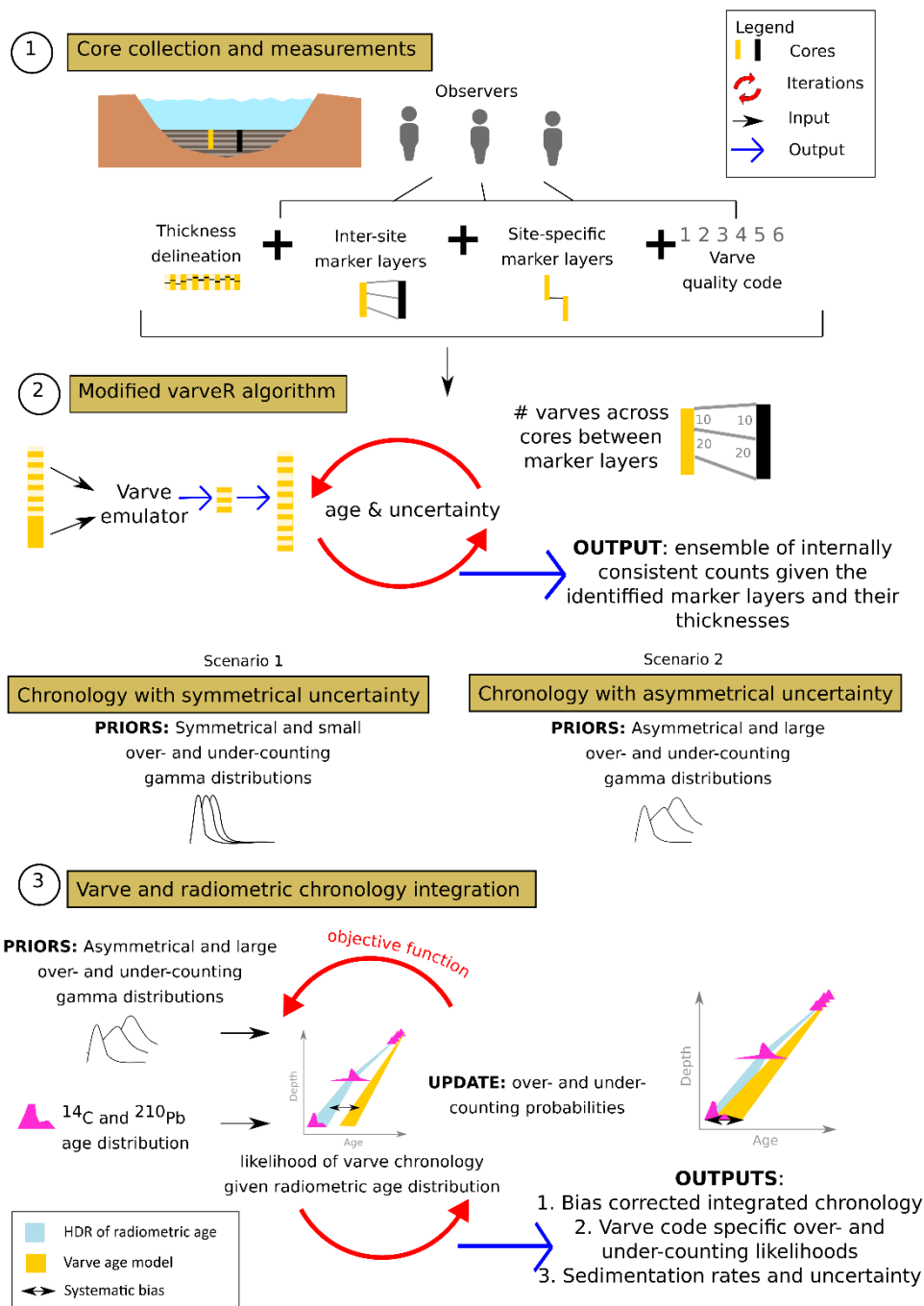
3.8 Varve chronology verification

255 A varve-based age-depth determination should be cross-checked with other independent dating methods to (1) support the
interpretation of varves as annual and (2) to identify systematic errors (Ojala et al., 2012; Zolitschka et al., 2015). To do so,
the varveR and integrated model output is depth-calibrated and displayed as age-depth curves. Then, the near-surface counts
are compared to radionuclide (^{137}Cs and ^{210}Pb) based age-depth models that use conventional CRS and CFCS and Plum, a
Bayesian approach to ^{210}Pb dating (Sec. 3.4). The full sequence is compared to a Bayesian radiocarbon age-depth model. All
260 comparisons are made using the dated core (COL17-3).

3.9 Varve and radiometric chronology integration

Bayesian statistics provide the opportunity to combine different chronological data and their uncertainty (e.g. Buck et al.,
2003) as well as information regarding the sedimentation process (e.g. Blockley et al., 2008) by informing priors (Brauer et
al., 2014). Here we use Bayesian learning to update prior estimates of the counting uncertainties for each observer given the
265 constraints from the independent radiometric model. Then, we combine the model into a master chronology.

Our Bayesian framework uses a custom Gibbs sampler to improve on the prior estimates of likelihood probabilities of over-
and under-counting described for the varveR model. The Gibbs sampler is initialized using the prior estimates of over- and
under-counting used in asymmetrical varveR (Fig. 2b). The sampler updates using an objective function that calculates the
270 likelihood of a proposed varve chronology given the radiometric ages and their probability distributions. We assume the
probabilities associated with varve quality codes 1 and 2 are best described using gamma distributions and must fall between
0 and 1. For algorithmic efficiency, we loosely impose the assumption that proposed adjustments that increase over-counting
rates should be balanced by decreases in under-counting rates, although overall reductions in both over- and under-counting
are possible and do occur. The output of the log objective function is the product of the age probabilities of all radiometric
275 samples and the over- and under-counting likelihood of all varve quality codes. The higher the output value, the closer the
improved varve count is to the maximum likelihood of the product of the radiometric ages. The Gibbs sampler innovates on
the previous over- and under-counting probabilities with each iteration if by adjusting with a small random number from a
normal distribution if there is an improvement in the output of the log objective function (i.e. a higher value). We ran the
Bayesian algorithm independently for each of the three observers until the objective values stabilized (~100 iterations), then
280 removed the burn-in and thinned the parameter chain to keep 1000 values. Finally, for each observer, we select the
parameters corresponding to the 300 highest objective values and combine them into combined posterior distributions. These
posterior distributions on the counting rates are then used to drive an updated varveR model and produce a master
chronology that effectively combines the radiometric model and the varve measurements from all observers (Fig. 3).



285 **Figure 3. Schematic of the approach used in this study. (1) Gathering raw measurements of varve thickness, counts, and marker layers for each core and each observer. (2) Using a modified version of varveR to produce a chronology following scenario 1 (symmetrical and literature-derived likelihoods of over- and under-counting) and scenario 2**



(asymmetrical and larger likelihoods of over- and under-counting). (3) Integrating radiometric information into the varve chronology by updating the prior likelihoods of over- and under-counting in an objective function. The posteriors of the n th best function output are used to run varveR and produce the final chronology that minimizes systematic bias and quantifies uncertainty related to misidentifying marker layers, observer bias, and varve quality and outputs sedimentation rates with uncertainty.

4 Results

4.1 Sediment profile

295 Columbine Lake sediments were previously described generally by Arcusa et al. (2019) and more detail is provided here. The sediments contain five stratigraphic units composed of minerogenic, laminated silts and clays ranging in color from grey to reddish-brown to orange (Fig. 4 and Fig. 5). Three of the four cores showed identical sediment profiles, but only COL17-2 and COL17-3 captured an intact sediment-water interface and laminations (Appendix A Fig. A1).

4.1.1 Units 5 and 4

300 Unit 5 (141-126 cm; depths in core COL17-2) is characterized by massive grey clay-sized sediment and lithogenic indicators (Si, Ti, K, Al, Rb, MS) are typically high and covary (Appendix A Fig. A4, A5 and A6). Unit 5 contained missing data so could not be included in the PCA (Fig. 5). The transition between units 5 and 4 is marked by a large and rapid increase in the redox element Mn, along with an instantaneous increase in Mn/Fe (Appendix A Fig. A5). Unit 4 (123-108 cm) is the first unit to contain laminations and correspond to the most elevated Fe and P. This unit contains type 1 varves.

305 4.1.2 Unit 3

Unit 3 (105-75 cm) contains poor quality laminations frequently interspersed with indistinct sections. The sections of indistinct varve preservation generally correlate across the parallel cores, although are more prevalent in core COL17-2 (Fig. 4). Unit 3 is characterized by type 1 varves.

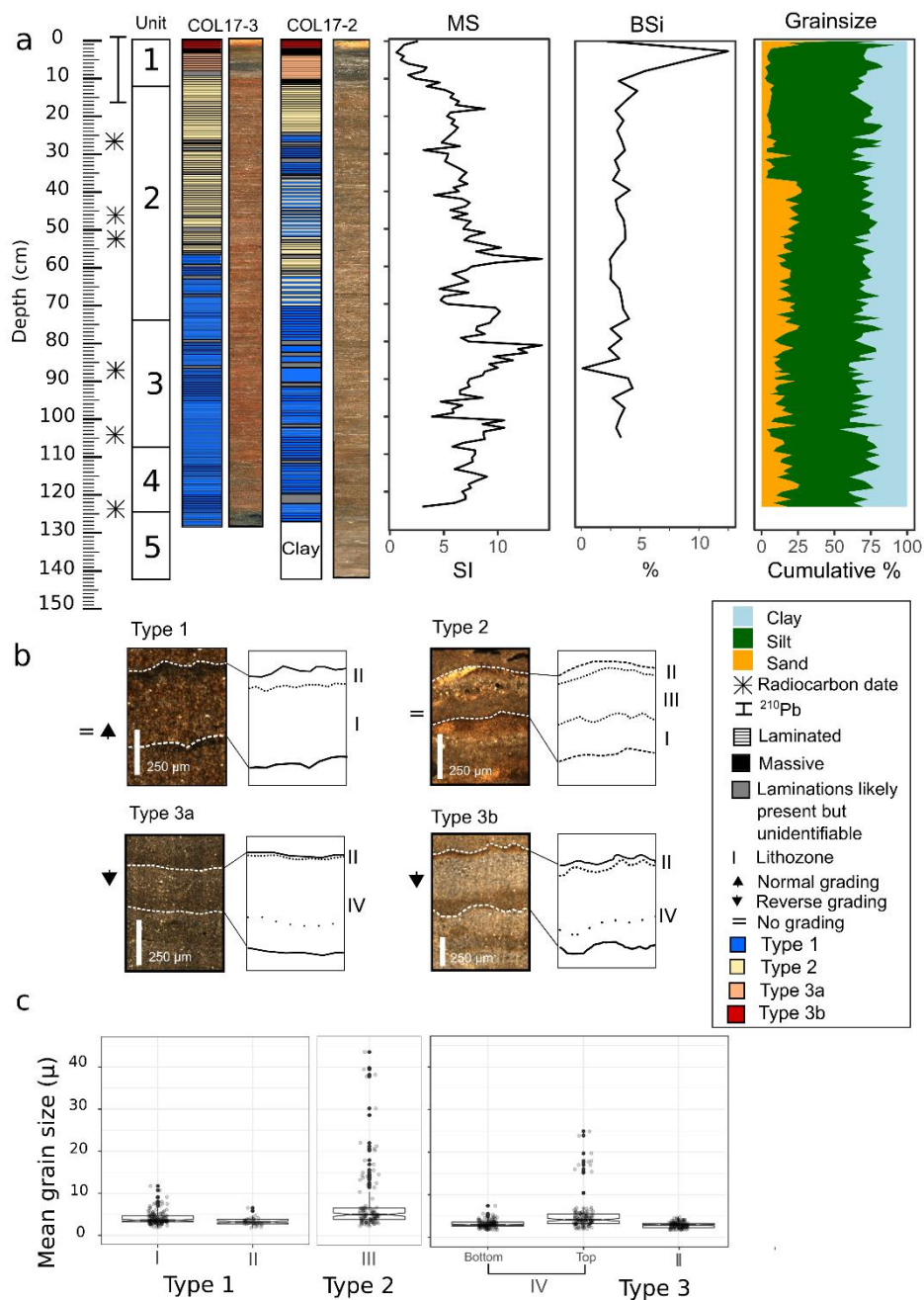
4.1.3 Unit 2

310 Unit 2 (72-12 cm) contains laminations of average clarity with indistinct sections (Fig. 4a). The sections of indistinct varves generally correlate across the parallel cores, with exceptions. Type 1 varves are present, although type 2 varves start to appear intermittently in core COL17-2. The break between units 3 and 2 coincides with a general shift from type 1 to type 2 that is evident both in the thin section microfacies analysis and the hierarchical clustering. Unit 2 sees a small but significant decrease in magnetic susceptibility and Fe compared to unit 3 (Appendix A A4 and A5).



315 4.1.4 Unit 1

320 This unit (12-0 cm) contains well-defined laminations as well as massive fine silt layers and can be further split into two sub-units. The lower sub-unit (12-2 cm) contains fine, grey, type 3a and b varves interspersed by two massive layers. The two massive light brown layers are both in core COL17-2, with core COL17-3 only containing the youngest of the two. Core COL17-3 contains a layer of indistinct laminations that cross-correlates with the oldest of the two COL17-2 massive layers suggesting the layers are composed of poorly preserved varves as opposed to single massive bed deposited rapidly. The other sub-unit (0-2 cm) contains thicker bright orange type 3b varves just below the sediment-water interface. Organic and biogenic (percent organics, biogenic silica, and green pigments as indicated by the index of RABD660) abundance increase to their highest levels in the top sub-section (Fig. 5, Appendix A Fig. A5), indicating increased lake productivity. Some heavy metals (Zn, Ag) also increase to their maximum levels (Appendix A Fig. A4).

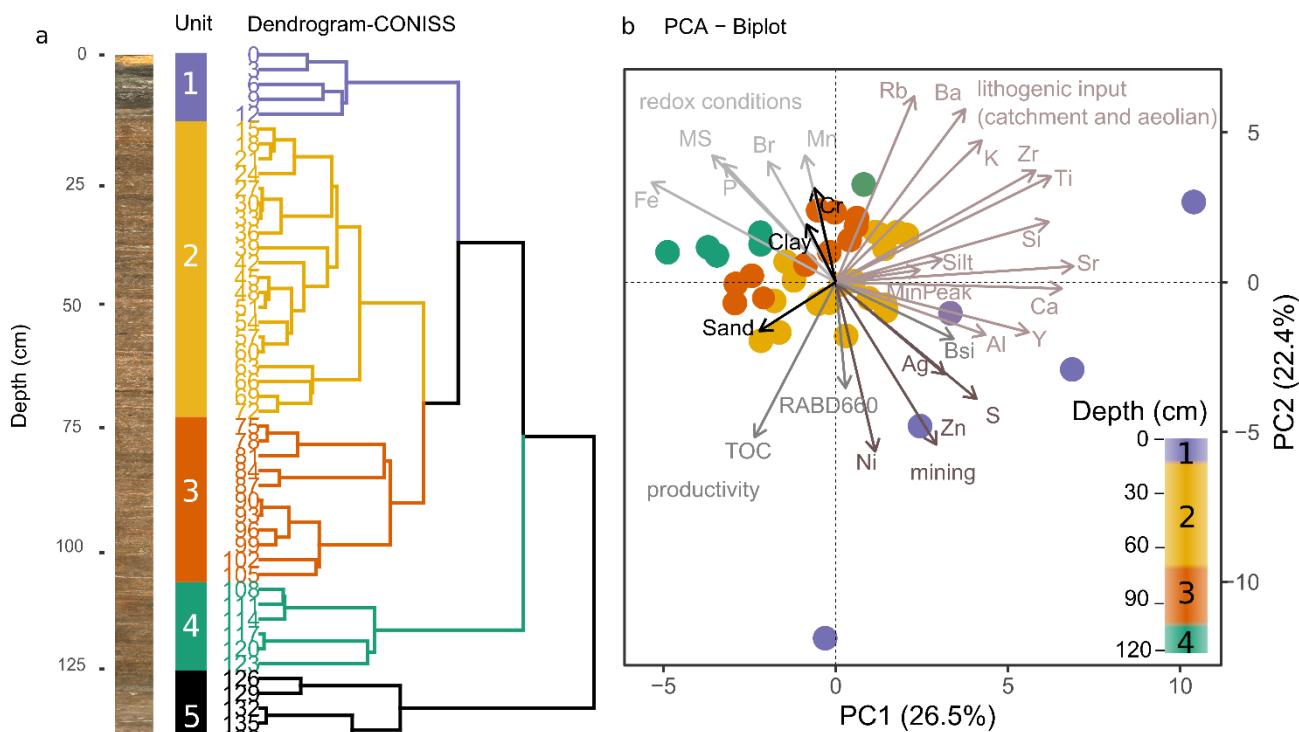


325

Figure 4. Sediment, proxy, and varve profiles. (a) Lithostratigraphy and location of radiometric samples of cores COL17-3 and COL17-2. Images are true color. The base of COL17-3 is black because the oxidized red crust has been scraped off. MS = magnetic susceptibility, BSi = biogenic silica. Other proxies are shown in Appendix A A5. (b)



330 Microscopic thin section examples of varve types 1, 2, and 3. (c) Microscopic sub-lamination grain size analysis of varve types 1, 2, and 3b.



335 **Figure 5. Statistical analysis of proxy data from core COL17-3. (a) A constrained dendrogram with significant clusters representing the stratigraphic units (1-5) color-coded and applied to the sample depths used in the (b) Principal Component Analysis (PCA) biplot for reference. The first two principal components explain 48.9% of the variability. PC variables grouped by indicator type have different colors. The image of the core is presented for context. PCA loadings and scores can be found in Appendix A Fig. A7.**

4.2 Varve type description

340 The examination of thin sections revealed complex microfacies that repeat within each lamination, indicative of a rhythmic change in the depositional environment. Moreover, comparison to radiometric measurements demonstrate this rhythmic layering is annual (Sect. 4.6). Therefore, the sediment is described here as true non-glacial clastic varves. Three main types of clastic varves are further sub-divided based on their internal structure (Fig. 4b). Type 1 is composed of typical couplets of silt and clay, type 2 couplets are interrupted by a third coarser grained sub-laminae, and type 3 couplets are inversely graded (Fig. 4c).



4.2.1 Type 1

345 Type 1, most common in the deepest half of the sequence, consists of couplets identified by color and grain size. The bottom part, lithozone I, is characterized by ungraded or fining upward grading of light reddish-brown sediment with grains that measure 5-15 μm (Fig. 4c). The top part, lithozone II, is a fine-grained, dark-brown clay-rich cap with grains consistently $< 5 \mu\text{m}$ (Fig. 4c). The contact between lithozones I and II is generally gradual.

4.2.2 Type 2

350 Varve type 2 is most common in the top half of the sequence and consists of couplets (lithozone I and II) interrupted by coarser-grained (25-40 μm) matrix-supported sub-laminae (lithozone III). An erosional contact separates lithozone I from III, which is composed of plagioclase, quartz, and oxides, as identified under polarized microscope light. Like type 1 varves, type 2 varves are terminated with a dark reddish-brown clay cap ($< 5 \mu\text{m}$, lithozone II).

4.2.3 Type 3

355 Type 3 varves are found exclusively at the topmost part of the sequence and can be sub-divided into varve type 3a and 3b. The deepest of the two, type 3a, is generally thicker and contains lithozone IV. Lithozone IV is characterized by a reverse grading of fine and dark grains at the bottom to coarse and light sediment at the top (Fig. 4c). Lithozone IV is followed by a thin and sometime non-existent lithozone II. Finally, at the topmost part of the cores is varve type 3b, similar in composition to varve type 3a. The difference is a strongly pronounced clay cap (lithozone II). Varve type 3 differs from type 2 because
360 the coarsest grains appear gradually within lithozone IV rather than abruptly in lithozone III. Lithozone IV in varve type 3a and b also gradually change in color from dark to light.

4.3 Varve counts, thicknesses, and quality

Varve thicknesses, excluding varves of quality code 4, 5, and 6, are similar for each core (Table 1), with a combined mean and standard deviation of 0.5 ± 0.05 mm. Thick varves were found in COL17-3. Varve quality was generally higher at the
365 top of the two cores (code 1) and fluctuated between moderate and poor quality throughout (Fig. 6).

With symmetrical varveR, cores COL17-2 and COL17-3 contain a total of 2466 (highest probability density region: 2075-2880) and 2380 (1999-2710) varves, respectively (Table 2, Fig. 7). This amounts to a cumulative uncertainty of $-391/+414$ varves ($-17/+15$ %) for COL17-2 and $-381/+330$ ($-17/+13$ %) for COL17-3. With asymmetrical varveR, the mean total varve
370 count increases by 300-400 varves to 2865 (1417-3923) for COL17-2 and 2740 (1394-3742) for COL17-3 although the cumulative uncertainty also increases to $-1448/+1058$ varves ($-68/+31$ %) and $-1346/+1002$ varves ($-65/+31$ %), respectively.



Table 1. Summary statistics for varve thicknesses based on the average of all observers' measurements, excluding intervals of indistinct laminations. Total varve counts indicate output of symmetrical varveR.

Core	COL17-2	COL17-3
Length of varved sequence (cm)	127	123
Mean total varve count	2466	2380
Median varve thickness (mm)	0.43	0.47
Min. varve thickness (mm)	0.04	0.05
Max. varve thickness (mm)	2.81	4.50
Mean varve thickness (mm)	0.49	0.52
Standard deviation varve thickness (mm)	0.28	0.29

375

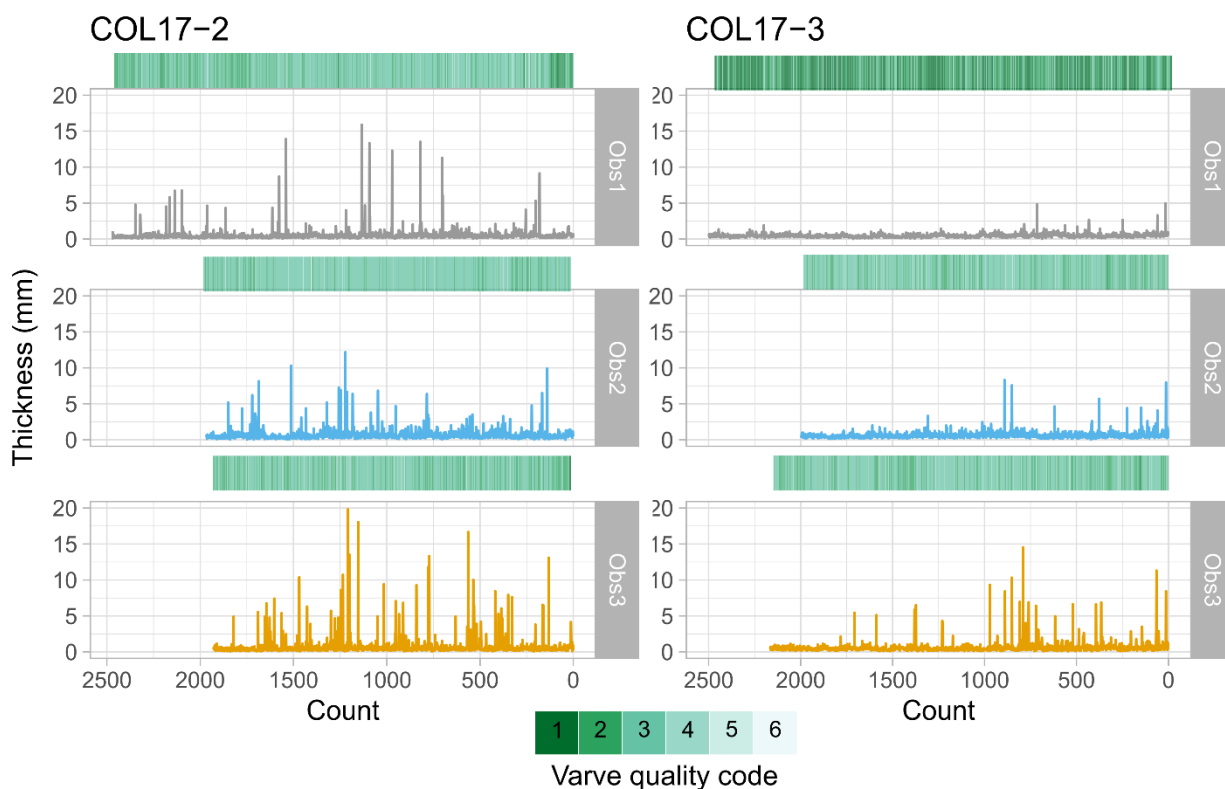


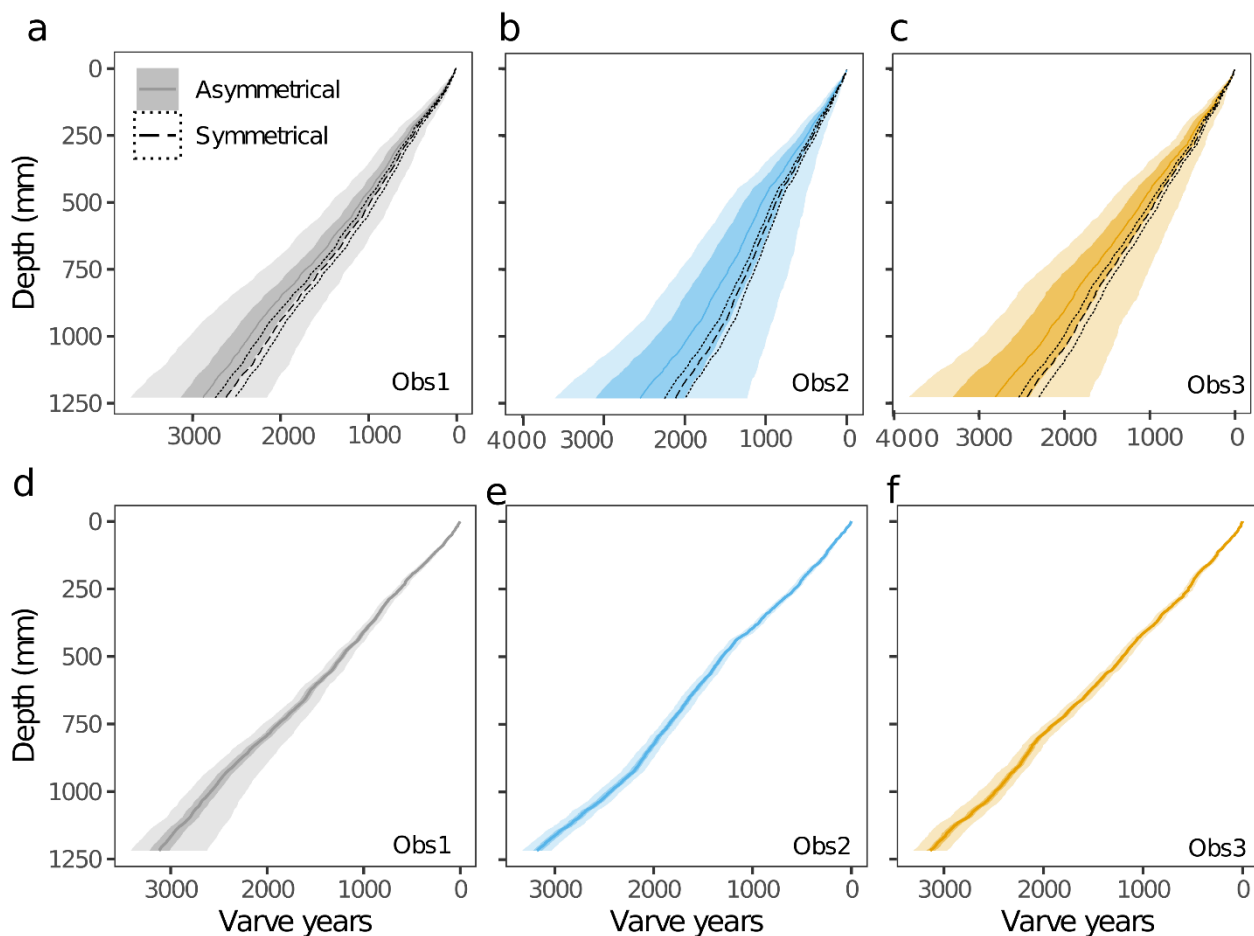
Figure 6. Observer measurements of varve thicknesses (lines) and quality (heatmaps) for cores COL17-2 and COL17-3.



Table 2. Comparison of observer and core-specific varve ages based on symmetric and asymmetric varveR as well as the integrated model. HDR = highest probability density region.

	COL17-2			COL17-3				
<i>Symmetrical varveR</i>	Obs 1	Obs 2	Obs 3	Average	Obs 1	Obs 2	Obs 3	Average
Ensemble mean total count (varve years)	2749	2171	2478	2466	2616	2103	2419	2380
HDR (2.5-97.5%)	2614- 2911	2037- 2320	2351- 2617	2033- 2847	2498- 2739	1958- 2249	2283- 2543	1999-2710
Difference from average (%)	+10.9	-12.7	+0.5	23.6*	+9.4	-12.4	+1.6	21.8*
<i>Asymmetrical varveR</i>								
Ensemble mean total count (varve years)	3107	2590	2898	2865	2899	2506	2813	2740
HDR (2.5-97.5%)	2015- 4182	1233- 3733	1756- 3864	1417- 3923	2161- 3717	1227- 3595	1699- 3811	1394-3742
Difference from average (%)	+8.1	-10.1	+1.1	18.2*	+5.6	-8.9	+2.6	14.5*
<i>Integrated model</i>								
Ensemble mean total count (varve years)	3470	3309	3227	3308	3095	3178	3138	3137
HDR (2.5-97.5%)	3098- 4075	3139- 3493	3091- 3370	3091- 3970	2624- 3414	3036- 3333	2968- 3309	2753-3375
Difference from average (%)	+4.8	0	-2.5	7.3*	-1.3	+1.3	0	2.6*

*) Indicates the observer agreement as the range in the percentage difference from the mean



385 **Figure 7. Comparison of original counts by (a and d) observer 1, (b and e) observer 2, and (c and f) observer 3 for dated core COL17-3. In the top row, the modeled varve counts are shown when using symmetrical (dotted envelop) and asymmetrical (shaded envelop) priors. For the symmetrical uncertainty, the median (dashed line) and the 97.5% (dotted region) high density regions are depicted. For the asymmetrical uncertainty, the median (darkest line), 75 (darkest shaded region), and 97.5% (lightest shaded region) high density regions are depicted. In the bottom row, the integrated varve and radiometric models are shown.**

4.4 Observer-related uncertainty

390 Three observers independently measured the varves of cores COL17-2 and COL17-3 in three separate transects (Table 2). The cumulative uncertainty of each observer to the mean was slightly higher for asymmetrical than symmetrical varveR. The uncertainty varied between 0.5 % (observer 3 COL17-2) and 12.7 % (observer 2 COL17-2). Asymmetrical varveR suggests more under-counting for observers 2 and 3 and more over-counting for observer 1 (Fig. 7). However, segment differences



are both positive and negative for all observers, indicating that systematic bias may not be an issue (Appendix A Table A1). The observer agreement is high for minimum thickness but low for maximum thickness (Appendix A Table A2). Observers
395 disagreed on the number of indistinct sections, pointing to the subjectivity of varve delineations and confidence levels. Agreement on varve quality between observers is low (Fig. 6), indicating further subjectivity. Sections with thicker varves generally correlate across all observers such as between the varve years of 0-100 and 750-1000 in COL17-3 or between the varve years of 1000-1500 in COL17-2 (Fig. 6).

4.5 Marker layer uncertainty

400 As marker layers were assigned by each observer individually, they may not agree between observers. Thus, the varve count between marker layers, or segment count, in each core indicates a combination of inter-site variability due to the sediment quality and observer judgment (Appendix A Table A1). The largest segment difference was 110 % (172 years) for one observer which cannot be explained by marker layer misidentification alone. Instead, it is indicating that one observer identified more indistinct sections than the other observers for one of the sites.

405 4.6 Independent validation

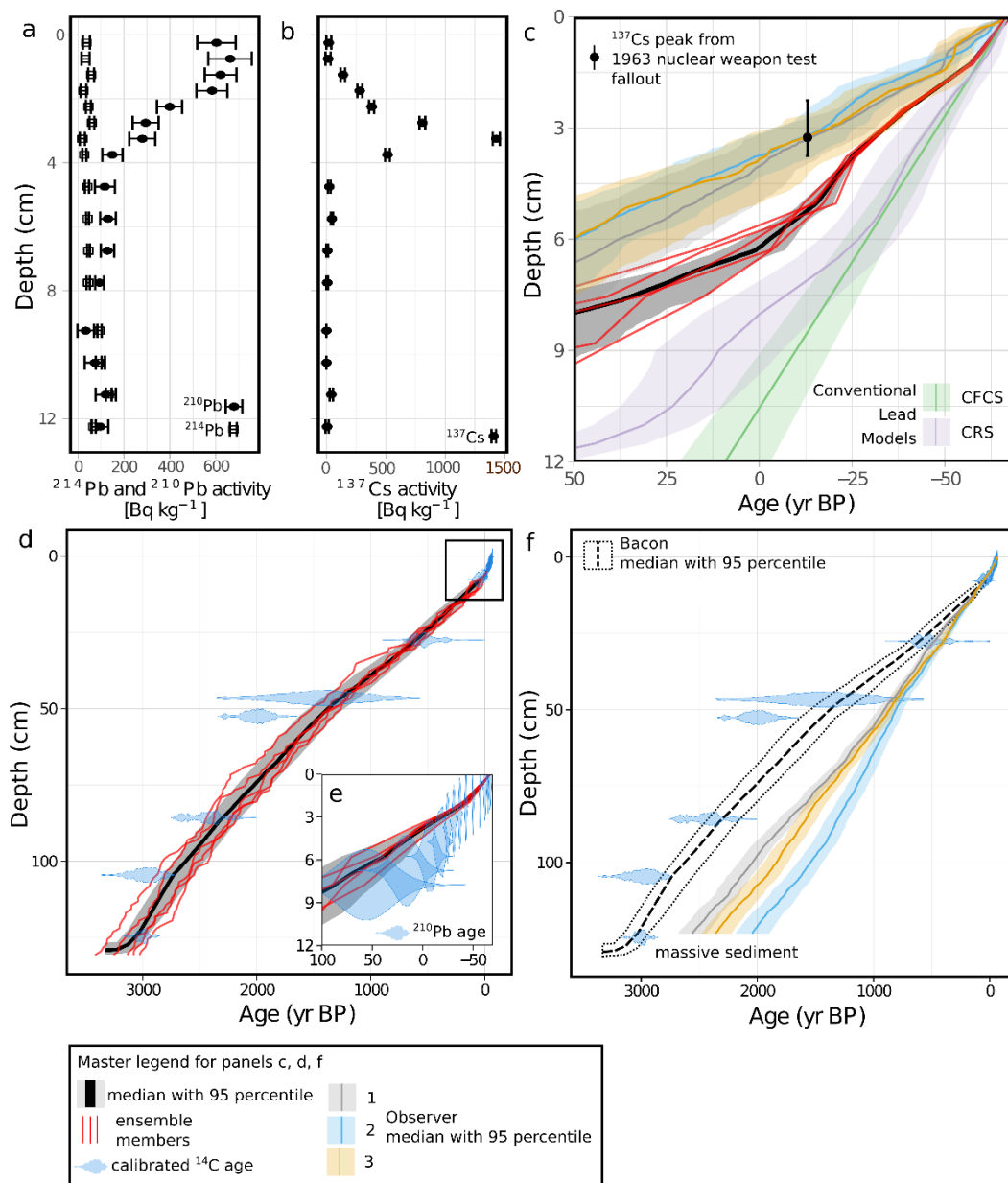
The topmost part of core COL17-3 was dated with two independent radionuclide profiles. The ^{210}Pb activity in Columbine Lake exhibits a gradual downcore decline that reaches equilibrium around 50 Bq kg^{-1} below 8 cm (Fig. 8a). The age at the base of the radionuclide measurements (12 cm) modeled by conventional methods for CRS and CFCS vary widely (Fig. 8c): CRS reaches $1883 \pm 14 \text{ CE}$ whereas CFCS comes to $1940 \pm 13 \text{ CE}$. In comparison, the Bayesian solution has a wider, but
410 likely more realistic uncertainty at 12 cm yielding a median age of 1784 CE with a 95 % highest density region of 1866-1679 CE. The ^{137}Cs activity shows a single peak at 3.25 cm (Figure 4.8B) which we attribute to the 1963 CE fallout from nuclear weapon testing. The peak's depth appears younger by 20 to 30 years in the ages modeled from the lead profile: CRS indicates a year of 1996 CE, for CFCS it is 1998 CE, and 1984 CE for Plum.

415 A total of six radiocarbon dates were used to model the age profile of Columbine Lake sediment (Table 3). Three dates were previously reported by Arcusa et al. (2019) (UCI 196901, UCI, 190157, and UCI 188317) for a mixture of small insects and plant fragments dated with a calibrated-age uncertainty ranging from 20 to 310 years. One new date was discarded as it returned a modern age (IonPlus 3528). Two more dates (IonPlus 3529 and IonPlus 3530) were measured on a mixture of plant fragments, bark, and aquatic insects due to the paucity of organic material found in the sediment. The uncertainty of the
420 two new dates ranged from 72 to 76 years. The calibrated basal age at 124.5 cm is 2997 (95.4 % probability: 3073-2888) yr BP.

To verify the annual nature of the couplets in Columbine Lake, we compare the topmost part of the varveR model with symmetrical priors to the ^{137}Cs chronomarkers and the entire sequence to the radiocarbon profile (Fig. 8c and f). Cesium-137



425 is used for comparison because of its lower uncertainty, as opposed to the lead age models which are not in close agreement
among themselves. The varve count and uncertainty by all three observers show a high agreement with the ^{137}Cs peak,
suggesting the couplets are annual. The whole sequence agrees generally well with the radiocarbon profile, particularly in
the top 25 cm. Uncertainty surrounding the varve count increases downcore and the varve counts no longer overlap with the
radiocarbon uncertainty to a depth of 60 cm. The basal radiocarbon age is older than the mean age estimated by both
430 symmetrical and asymmetrical varveR by 600 and 250 years, respectively. The cumulative uncertainty of asymmetrical
varveR encompasses the radiocarbon basal age, whereas the symmetrical varveR does not. Counts from observer 1 are
systematically closer to the radiocarbon age estimate. The comparison with radiocarbon also serves to identify systematic
biases which in the case of Columbine Lake varves tend towards under-counting when using symmetrical priors and possibly
over-counting when using asymmetrical priors.



435

Figure 8. The chronology of Columbine Lake core COL17-3 based on (a) lead and (b) cesium measurements is seamlessly combined with (c, d) radiocarbon samples using the Bayesian models of Bacon and (e) Plum. Plum performs better than (c) conventional lead models of CFCS and CRS when compared to the 1963 ¹³⁷Cs fallout peak. The age-depth models counted by three observers and modeled by varveR with symmetrical priors agree well with the fallout peak indicating the rhythmic laminations are annual. Compared to (f) radiocarbon, underestimations in the varve counts appear to accumulate downcore.

440



Table 3. Uncalibrated and calibrated radiocarbon dates.

Lab ID	Depth ^a (cm)	Material	¹⁴ C Age (¹⁴ C yr BP)	Error (± 1sd yr)	From ^b (cal. yr BP)	To ^b (cal. yr BP)
UCI 196901	27.5	Insect wing	520	100	671	319
UCI 190157	46.5	Bryophyte twig, Daphnia ephippia	1510	310	2146	790
IonPlus 3527	52.5	Daphnia ephippia, insect armour	2045	69	2299	1798
IonPlus 3528 ^c	77.75	Daphnia ephippia, charred twig	-935	60	-	-
IonPlus 3529	85.75	Daphnia ephippia, charcoal	2365	72	2710	2160
IonPlus 3530	104.5	Daphnia ephippia, bark	2845	76	3170	2777
UCI 188317	124.5	Bryophyte twig, Daphnia ephippia	2875	20	3073	2888

^a Mid-point depth of 1-cm-thick sample

^b Two sigma range calibrated with IntCal20 curve

^c Age not used because returned modern

445

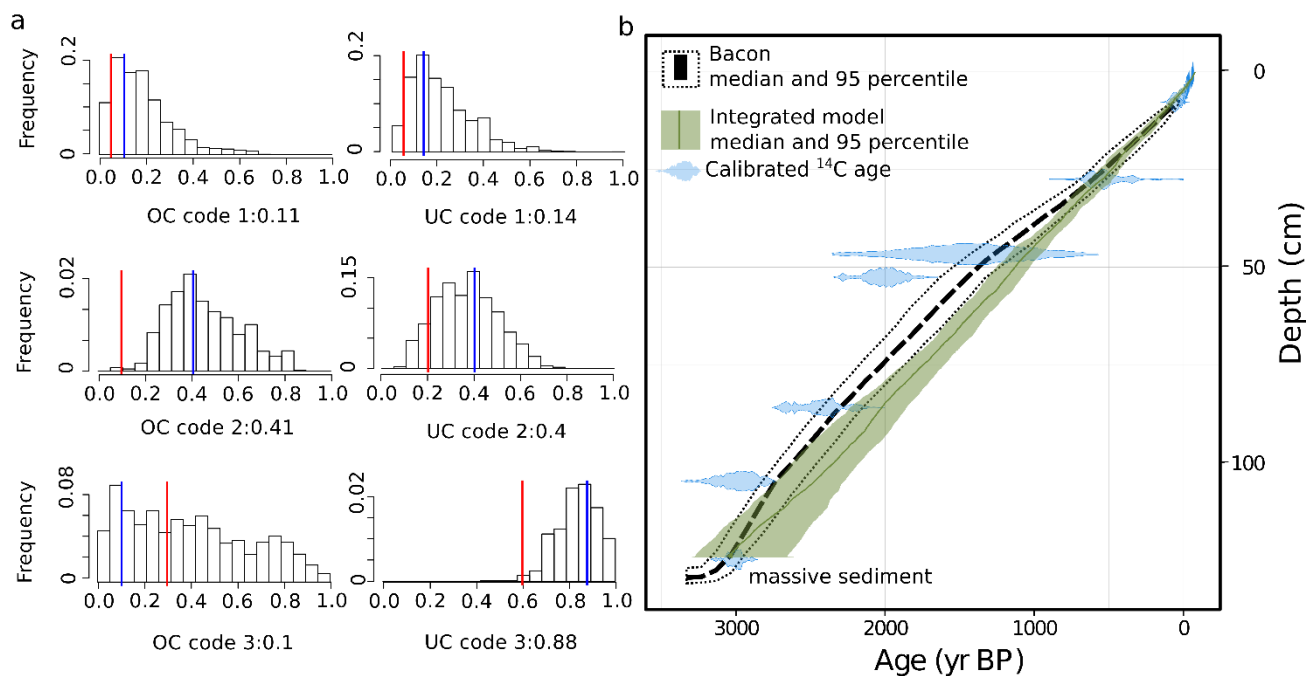


4.7 Varve and radiometric data integrated model

One integrated model was created for each observer. The integrated models updated the prior estimates of the counting uncertainties given the constraints from the independent age model and given each observer's varve thicknesses, varve quality designation, and marker layer identification. The models sampled the probability space for 50,000 iterations and the
450 burn-in occurred rapidly in <100 steps (Appendix A Figure A8). The integrated models result in similar cumulative uncertainty to symmetrical varveR but are much smaller than the uncertainty estimated by asymmetrical varveR (Fig. 7). The integrated models also converge more: the difference in the basal age between observers shrinks to 2.6 %, down from 21.8 % in the symmetrical varveR. The posterior likelihoods of over- and under-counting are larger than the symmetrical priors (Fig. 2 compared to Appendix A Figure A9). They also varied with each varve quality code and with each observer (Appendix A
455 Figure A9). The integrated models were more successful at correcting for over- and under-counting for observers 2 and 3 than observer 1 as seen from the more symmetrical cumulative uncertainty for those observers (Appendix Fig, A8).

Each observer's integrated model was combined into one single integrated model, which hereafter is referred to as the 'integrated model'. The integrated model cumulative age extends by 3137 (3375-2753) varve years or 1120 (1358-736) BCE
460 corresponding to a cumulative uncertainty of -384/+238 years (-13/+7 %) (Table 2). The cumulative mean age is older than symmetrical and asymmetrical varveR and the independent model. However, the HDR encapsulates the mean age of the radiometric mode (Fig. 9b). The greatest deviation between the independent model and the integrated model occurs between 30 and 80 cm depth where indistinct sections are most frequent (Fig. 9b). The cumulative uncertainty in the integrated model is lower than asymmetrical varveR and similar to the symmetrical varveR.

465 The posterior probabilities of over- and under-counting are higher than the prior expectations for all varve quality codes except for the likelihood of over-counting code 3 (Fig. 9a). The probability of over- and under-counting is similar for varve code 1, with a slight tendency for more under-counting (11 % vs 14 %). Furthermore, the probability of over- and under-counting varve code 2 is the same (41 % vs 40 %). In contrast, the likelihood of over-counting varve code 3 is much smaller
470 than the likelihood of under-counting (10 % vs 88 %). However, the distribution of the likelihood of over-counting is much wider than for other varve quality codes indicating this parameter has the least influence on the iterative improvements made by the Gibbs sampler. More under-counting appears with deeper sediment due to the dominance of poorly preserved sediment identified as varve quality code 3. Similar posterior probabilities resulted from re-running the integrated model with smaller asymmetrical uncertainty.



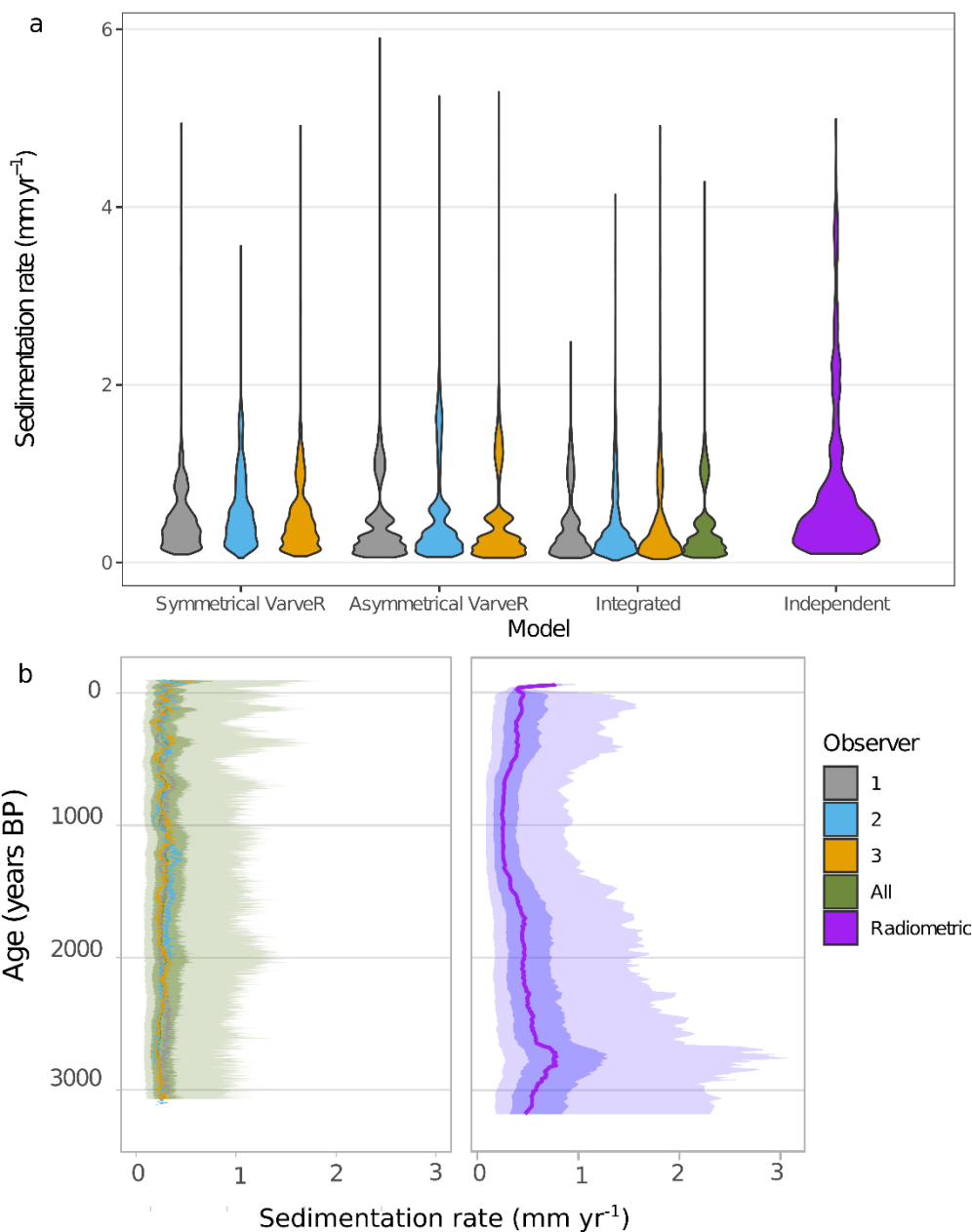
475

Figure 9. Integrated varve-radiometric mode. (a) Over- and under-counting posterior distributions for the integrated model for each varve quality code (1, 2, 3). (b) Age-depth model comparison of the independent (Bacon) age model and the integrated model. OC: over-counting. UC: under-counting. Blue line indicates the mode of the posterior distributions. Red line indicates the mode of the prior distributions.

480 4.8 Sedimentation rates

The estimated sedimentation rate and its uncertainty varied by method and observer (Fig. 10a). Average rates are similar for all varve models with estimates of 0.51 mm/yr (HDR: 0.12-1.45) in symmetrical varveR, 0.44 mm/yr (HDR: 0.08-1.76) in asymmetrical varveR, and 0.42 mm/yr (HDR: 0.08-1.30) in the integrated model. In contrast, rates are doubled on average and higher more frequently in the independent model (0.83 mm/yr, 0.11-3.63) (Fig. 10). The uncertainty range in the varve
485 models is half of that in the radiometric model.

Sedimentation rates appear more stable throughout the late Holocene in the integrated model than for the radiometric model (Fig. 10b). Periods of higher sedimentation rates occur in the integrated model in the last 100 years, 400-500 BP and 2000-2200 BP. Only the last 100 years of the integrated model shows a similar although subdued trend to the radiometric model.
490 Furthermore, sedimentation rates are highly sensitive to the observer measurements with relatively little agreement (Appendix A Fig. A10). Those periods of agreement would show lower uncertainty, but uncertainty is relatively stable throughout the record (Fig. 10b).



495 **Figure 10. Comparison of sedimentation rates. (a) Summary of sedimentation rates calculated with different models and separated by observer. (b) Late Holocene median (thick lines), 75% (darker shading) and 97.5% (lighter shading) highest probability density regions estimates of sedimentation rates calculated by the integrated (left) and radiometric (right) models for the dated core COL17-3. Note the medians of each observer are plotted in the left panel (thick lines).**



5 Discussion

500 5.1 Sources and quantification of uncertainty

Varve chronologies, like all sedimentary profiles, contain uncertainties that stem from complex internal structures, poor quality, technical problems, rapid deposition events, and erosion (Ojala et al., 2012). Unlike other sedimentary chronologies, the errors are propagated by the observer(s) who somewhat subjectively determine what is a varve by “lumping” or “splitting” thicknesses. The sources of uncertainty and their quantification in Columbine Lake are now discussed in turn.

505 5.1.1 Sediment microstructures

The combination of the complex internal structure, shifting structures through time, and thinness of Columbine Lake varves was likely the most important source of uncertainty (Fig. 4b, Sect. 4.2). The complex sub-lamina internal structures the clastic varves are the primary cause of the large uncertainties in observer identification and delineation. It is also likely that laminations are missing due to erosion. Both would result in the under-counting that is particularly evident when comparing
510 the symmetrical and asymmetrical varveR models to the independent chronology (Fig. 8). The systematic bias is corrected by the integrated model. Additionally, uncertainty in the varve delineation impacts the thickness measurements which propagates into the sedimentation rates (Fig. 10). At an average thickness of 0.5 ± 0.05 mm, the uncertainty surrounding the delineation of each varve is likely to be proportionately large because of the image quality and pixel resolution used in this study. Missing laminations and misinterpretation due to complex varve structures are common reasons for imprecision
515 (Ojala et al., 2012).

5.1.2 Sediment quality

Closely intertwined with the sediment microstructures, sediment quality is likely the second-most important source of uncertainty in the chronology as seen from the prevalence of poor varve quality codes (2 and 3) (Fig. 6). About 78% of the sediment of COL17-2 and COL17-3 was identified as code 2, 3, and 4, all three designations indicating the observer was less
520 than 80 % certain the thickness delineated was accurate. We report a cumulative uncertainty ($-13/+7$ %) in the integrated model that is on the higher end of values reported in the literature: a cumulative uncertainty of $\pm 1-3$ % is reported in the literature for well-preserved sediment (Ojala et al., 2012) and up to 15 % for unclear, partially disturbed varves in otherwise well-preserved varve sequences (Ojala and Tiljander, 2003; Tian et al., 2005). We also find high estimates of probabilities of over- and under-counting. These uncertainties are not always quantified in the literature, but Ojala and Tiljander (2003)
525 report uncertainties within sections that reach 12 % and indicate more over-counting with depth. Additionally, Fortin et al. (2019) report over- and under-counting estimates of 21.9 and 14.5 %. We find large uncertainty estimates even for the best quality varves in Columbine Lake.



The presence of indistinctly laminated sections was frequently identified in both cores (Fig. 4). The timing of these segments is generally correlated across both cores, with exceptions, suggesting a combination of macro and micro scale processes. We accounted for this uncertainty through varve code 5 by emulating varved sediment. Through this analysis, we found that, on average, more sediment was identified as indistinctly laminated in COL17-2 (25 cm) than COL17-3 (11 cm). In more detail, the identification and thickness of these segments varied between observers suggesting differences in expert confidence and indicating high uncertainty may be surrounding the timing of these segments. As a result, the meaning of these indistinct segments should be interpreted with caution.

5.1.3 Technical errors

Technical errors in Columbine Lake varve chronology are likely limited to the sediment embedding and thin-sectioning process rather than the coring stage. All cores were remarkably similar (Appendix A Fig. A1), and layers could easily be correlated suggesting the coring process did not disturb the sediment. Although thin sections were overlapped to minimize sediment loss, the microscopic analysis revealed splits across the sediment in the middle of thin sections likely due to the embedding process. While infrequent, we accounted for the uncertainty associated with these gaps by using varve code 6, which tried to quantify the missing sediment. Varve code 6 added an average of 1.2 and 1.7 cm to COL17-3 and COL17-2, respectively. varveR provides a means of estimating this uncertainty.

5.1.3 Rapid depositional events

Errors associated with rapid depositional events were also likely limited to the topmost part of the record. Two thick layers were found in COL17-2 (1.2-2 and 8.5-9.7 cm) and one in COL17-3 (1.5-2.5 cm). The oldest of the two layers in COL17-2 corresponds to a section of indistinct laminations in COL17-3 (7-8 cm). In situations where one core contains rapid depositional events, but the other does not, varveR attempts to correct for the missing varves by using information from both cores. In the case of the oldest layer in COL17-2, only partial information was available from the other core (COL17-3) because of the indistinct laminations. As a result, information was filled in by the varve emulator which assumed that varves should be present at that depth. This assumption is likely valid in this case but highlights the emulator should be used with caution.

5.2 Varve formation mechanism

Clastic varves generally form in lakes with (1) favorable catchment properties, lake bathymetry, and hydrology, (2) an absence of sediment mixing, and (3) a seasonally variable and significant flux of different components (Anderson et al., 1985; Ojala et al., 2012; Zolitschka et al., 2015). Due to its remarkably clear water and popularity as a backcountry hiking destination, we could not obtain permitting to instrument Columbine lake to monitor sediment deposition. Therefore, our understanding of its non-glacial clastic varve formation mechanism is based on field observations, satellite imagery, and proxy data. Weather data from the region also inform this understanding.



560

Non-glacial clastic varves form in catchments containing fine-grained silt and clay material, where at least one inflow is present, and where the bathymetry is deep compared to the surface area (Ojala et al., 2000; Zolitschka et al., 2015). In Columbine Lake, most of the catchment (96%) is unvegetated (Arcusa et al., 2019). The production of siliciclastic fine-grained material is likely dominated by the freeze-thaw cycle and hydrolysis. The eroded material is then entrained into the lake from the margins and via an inflow located to the northwest (Fig. 1). An older inflow is visible from satellite imagery just south of the modern inflow that may also activate during wetter periods. Upon entering the lake, coarser grains settle out first as the energy dissipates and the finer material reaches the coring site. The relatively deep pocket (27 m) where the coring site is located fits the description of a plain sediment depression (Ojala et al., 2000), where depth allows for anoxic conditions and continuous sedimentation and width prevents slope slumping and episodic turbidity currents (O'Sullivan, 1983).

570

The absence of sediment mixing, crucial for varve formation, generally relates to conditions that deter bioturbation (Anderson et al., 1985; Zolitschka et al., 2015). Perennial anoxia, or meromixis, or situations where oxygenation is infrequent enough to deter organism establishment are typical conditions. The deep plain depression where the coring sites are located likely contributed to this condition, although instrumental data of the water column is unavailable to check for anoxia. Moreover, acidic lake water (pH 5) may be an additional deterrent to benthic biota.

575

The seasonal sediment transfer in an alpine non-glaciated catchment is usually related to the annual freeze-thaw cycle and runoff events (e.g. snowmelt and rainfall) (Zolitschka et al., 2015). Three types of clastic varves are found in Columbine Lake with distinct structure, and understanding their formation requires separate mechanisms. Clastic varves are typically composed of a coarse-grained lower and a fine-grained upper lamina produced by a nival discharge followed by winter settling (Zolitschka et al., 2015). Such a progression is found in Columbine Lake's type 1 varves, but not type 2 nor 3. Like previous studies (Cuven et al., 2010), we interpret the type 1 varves silt base (lithozone I) as deposition during the snowmelt season and the clay top (lithozone II) to the settling of fines under ice cover. Two mechanisms can produce the structure of lithozone I. One possibility is that in the first weeks of snowmelt, the frozen ground and riverbanks inhibit sediment transportation. The resulting stream with low sediment concentration produces overflow conditions. Once in the distal basin, the sediment settles rapidly in ungraded or fining upward sequences (Francus et al., 2008). Alternatively, the initial melt release may occur before the stratification of the lake (Palmer et al., 2019). Either way, we interpret type 1 lithozone I as low-energy, low sediment concentration, nival discharge. The gradual contact between the lithozone I and II may indicate a slow shut down of turbulence by a slow freeze over and a prolonged period of settling (Desloges, 1994). The sharp contact between lithozone II and the following lithozone I possibly represents the erosive waxing head of the flow, even if the flow is low-energy (Mulder et al., 2001).

585

590



In contrast, type 2 varves are composed of subparts that do not follow the typical silt-to-clay progression. The transition from lithozone I interpreted as low energy nival discharge to lithozone II that is interpreted as winter settling is often interrupted by lithozone III, a coarse sub-lamina. The combination of lithozone I and III gives the impression of a single sub-laminae with reverse grading. However, because an erosive contact is sometimes evident between lithozone I and III, this interpretation is likely ruled out. Instead, a second possible explanation is a high-energy event occurring during or after snow melt but before freezing over. The San Juan Mountains experience a bimodal precipitation regime with abundant snow in the winter followed by violent summer thunderstorms. These short-lived summer events may have the energy to transport coarser material than during the nival snowmelt. As identified in other settings (Cuven et al., 2010), we interpret lithozone III as discharge events produced by high-intensity rainfall occurring during or after the spring melt.

In varve type 3, lithozone I is replaced with lithozone IV. Rather than a coarse event interruption like lithozone III, lithozone IV is composed of a single lamina with an inversely graded transition from a dark and fine bottom to light and coarse top (Fig. 4c). Inversely graded sediment has only rarely been described in lake sediment (Desloges, 1994; Francus et al., 2008; Guyard et al., 2007; Lewis et al., 2010; Palmer et al., 2019). The primary suggested deposition mechanism is the increasing underflow velocity of a hyperpycnal flow during the initiation of a flood (Gilli et al., 2013; Lamb and Mohrig, 2009; Mulder et al., 2001). This depletive (slower velocity with distance) waxing (increasing velocity with time) flow generated by the steadily increasing discharge (rising limb) at a river mouth (Kneller, 1995) has been attributed to secondary pulses of sediment in the summer (Desloges, 1994), variable flow from precipitation events (Lewis et al., 2010), and lateral flow of the sediment to the core site (Palmer et al., 2019). Although possible, this mechanism would require specific discharge rates and sediment concentrations to produce a current that increases in velocity to a critical discharge rate and is denser than the lake water in which it enters (Mulder and Syvitski, 1995).

An alternative hypothesis to explain the inversely graded sediment is specific to Columbine Lake and builds on the evidence of dust-sized sediment in the coarse top of lithozone IV (particle size 5-25 μm). A previous study of Columbine Lake demonstrated that mineral dust transported from the Southwestern deserts make up 30-57% of the sediment (Arcusa et al., 2019). As the mode grain size of the dust (22 μm ; Neff et al., 2008; Routson et al., 2016) falls within the grain size range of the top of lithozone IV (Fig. 4c) and dust is regularly found settled on snow in the catchment and on the frozen lake surface (Appendix A Fig. A11), it is conceivable that the coarse top of lithozone IV would be composed of dust brought into the lake in one or a combination of three ways. First, dust can accumulate on the lake ice cover and be released as the ice melts, and this may be later than the onset of snowmelt from the catchment that would create type 1 varves. Second, as snow melts around the dust particles deposited in the catchment, the concentration of the dust left behind increases (Conway et al., 1996; Li et al., 2013). A precipitation event late in the nival season could eventually wash the dust into the lake creating the appearance of inverse grading. Third, the dust-sized material is not dust but catchment material the size of dust brought in from lake margins or the inlet late or at the peak of the nival season. Varve formation due to aeolian dust has been



documented previously (Zhai et al., 2006), but whether the inversely graded subparts are due to additions of dust and/or hyperpycnites is unclear from the evidence currently available.

630 5.3 Varve formation through the Late Holocene

Three transitions in the varve formation are evident from the stratigraphy and varve analysis. These transitions are either abrupt or gradual and likely reflect important changes in the catchment conditions and/or climate. These transitions will be discussed in turn, from oldest to youngest. Ages and their highest probability density regions (2.5-97.5 %) are indicated from the integrated chronology.

635

The most abrupt transition in the sequence occurs around 1120 (HDR: 1358-736) BCE (3137, 2753-3375 BP) with the onset of varve formation (Fig. 4) at the contact between units 5 and 4. The processes that can create and sustain conditions necessary for varve formation relate to the physical and chemical properties of the lake water that produce anoxic conditions. These factors include temperature, wind exposure, increased production, and decreased lithogenic influx (Boehrer et al., 2017; Butz et al., 2017; Makri et al., 2020). In the case of Columbine Lake, lithogenic elements (Ti, Ba, Rb, K) decrease, and Mn/Fe temporarily increases at the transition and is low thereafter (Appendix A Figures A4 and A5). When uncorrelated with detrital elements, as is the case here, high Mn/Fe has been interpreted as high dissolved oxygen concentration in the water column (Naeher et al., 2013). The cause for this momentary increase in oxic conditions is unclear but marks the beginning of the varve formation. Unit 4 directly follows this transition and redox conditions are consistently indicated by the PCA analysis (Fig. 5b).

645

The second most evident transition occurs around 60-50 cm depth in COL17-3 (as deep as 72 cm in COL17-2) corresponding to 419-882 C.E. in the integrated varve chronology model with the gradual shift from varve type 1 (unit 3) to 2 (unit 2) (Fig. 4 and Fig. 5). Whereas the asynchronicity of the transition in the cores suggests site specific causes (e.g. processes that oppose varve formation), the fact that both cores eventually transition indicates a catchment wide influence. The main distinction of varve type 2 is the presence of sub-laminae that are interpreted as higher-energy rainfall events. The position of these laminae within the lamination set suggests the precipitation event occurred late in the nival season, in summer, or in the fall but before the winter settling commenced. The timing of the transition corresponds broadly with the Dark Ages Cold Period (Helama et al., 2017) generally characterized by increased moisture in the southern Rocky Mountains (Rodysill et al., 2018; Routson et al., 2011) although a period of drought is recorded between 600-700 C.E. at Summitville, 110 km to the south east (Routson et al., 2011). Due to the asynchronicity the timing of the transition cannot be ascertained, and the climatic cause should be interpreted with caution.

655

The final transition occurs at a depth of 7 cm corresponding to an age of 1874 (1844-1902) C.E. The difference between unit 2 and 1 in the PCA analysis is striking (Fig. 5), with lithogenic inputs distinguishing unit 1 from unit 2. The transition from

660



unit 2 to 1 appears to occur after the deposition of the deepest massive layer (also a section of indistinct varves in COL17-3). As discussed in section 3.2.2, a large proportion of the sediment appears to be dust-sized sediment (Arcusa et al., 2019). Additionally, the last 150 years coincide with a 1.7-fold increase in dust deposition compared to pre-industrial times in the San Juan Mountains (Routson et al., 2019), with two peaks in deposition occurring around 1880 C.E. and 1950 C.E. as seen
665 from previous work at Columbine Lake (Arcusa et al., 2019) as well as other lakes in the region (Neff et al., 2008; Routson et al., 2019, 2016). These peaks correspond to the timing of the massive layers: 1973 (1959-1987) C.E. and 1851 (1824-1876) C.E. It is thus conceivable that the additional dust may have disrupted the varve formation process in the massive layer and may have altered the varve formation mechanism subsequently.

670 A final hypothesis for the transition to varve type 3 relates to an increasing, even if slight, human impact on the catchment as indicated by two structures and other evidence of grazing and mining activity (Fig. 5). Although the catchment is not accessible by road, a rock shelter was constructed on the south shore. The high alpine meadows have been subject to sheep and cattle grazing since the late middle to late 1800s (Baker, 2020) coinciding with the increased lake productivity indicators seen in unit 1 (Fig. 5). The increased productivity and organic content could explain the thicker varves but not the reverse
675 grading. Secondly, a 2-m-high dam was constructed at the outlet for Mill Creek presumably sometime around the turn of the 20th century, to raise the lake water level and secure water rights for a downstream mine (pers. comm., Forest Service at San Juan National Forest). This water level increase and fluctuation could have increased erosion and reworking of hillslope sediment. Finally, mining became increasingly prevalent in the area from the 1800s (Blair and Bracksieck, 2011), although we did not find evidence for mining within the catchment. Mining indicators (e.g. Guyard et al., 2007) such as silver and
680 zinc become abundant in unit 1, and the increase in heavy metals could have changed both lake productivity and signal a change in lithogenic input. Whether the unique varve type 3 reflects the input of dust or sediment from shoreline or hillslope sources, or changes in lake productivity, or all these factors together, the change occurs in the industrial period and is likely related to human activities within and beyond the catchment.

5.4 Integrating varves with radiometry

685 Radiometric (^{14}C , ^{210}Pb , ^{137}Cs) profiles are frequently used to validate varve chronologies (Ojala et al., 2012; Zolitschka et al., 2015); however, ages derived from radiometric profiles are generally systematically older than the varve chronology for various reasons (Bonk et al., 2015; Tian et al., 2005; Żarczyński et al., 2018). As the varveR output for Columbine Lake consistently shows this divergence (Fig. 8f) we now discuss the merits and pitfalls of integrating the varve chronology with the independent radiometric age-depth model by exploring three possibilities: (1) the varveR model is accurate and the
690 calibrated ^{14}C dates are older than the true sediment ages; (2) the calibrated ^{14}C dates are accurate and the varveR model underestimates the true sediment ages; or (3) both the model and the calibrated ^{14}C dates have unknown systematic biases.



Radiocarbon dating in high-elevation lake sediments is often challenged by a paucity of adequate organic material (e.g. Arcusa et al., 2020; Schneider et al., 2018). To gather enough material for a standard graphite-based AMS measurement, the radiocarbon samples in this study were composed of a mixture of aquatic and terrestrial material (Table 3). Samples of mixed composition have been shown to yield ages that are generally too old (Zander et al., 2019). Both aquatic and terrestrial macrofossils are associated with processes that can increase their apparent age. For example, aquatic organisms are subject to a hardwater effect due to dissolved inorganic carbon synthetization (Geyh et al., 1998, 1999), whereas terrestrial material might be significantly older than the enclosing sediment because of the lags between growth and deposition (Bonk et al., 2015). At least one of the seven radiocarbon dates is likely too old (IonPlus 3527), exceeding Bacon's 95 % uncertainty band (Fig. 8f). A leave-one-out cross-validation analysis (e.g. Parnell et al., 2011) could help identify other outliers but the analysis was not undertaken in this study. Despite the potential for other samples being too old, the integrated chronology overlaps with all other radiocarbon samples (Fig. 9b), and the divergence between symmetrical varveR and the radiometric independent model appear to increase with depth (Fig. 8f), both of which support the accuracy of the varve-based age model.

A younger varve chronology compared to the independent model would indicate varve under-counting. Varve count underestimation is recognized in sediment with poor varve appearance (Tian et al., 2005) and depending on the method used in building the chronology (Żarczyński et al., 2018). As discussed in section 5.1, both the sediment microstructures and the quality of the varve appearance are important sources of uncertainty in Columbine Lake: varves are thin, complex, and their formation mechanism appears to change through time. Additionally, the varve emulator is unlikely to have over-estimated the varve counts given the relatively stable sedimentation rate through time. Although observer bias does not appear important, since age deviations from the mean are both positive and negative, and for the reasons listed above, it is most likely that systematic under-counting is prevalent. The integrated model satisfies all available evidence and is more accurate than relying on a single chronological method.

6 Conclusion

A multi-core, multi-observer varve chronology extending 3137 (-13/+7 %) years was produced from thin and complex varves from high-elevation Columbine Lake, Colorado. A varve formation model was proposed and was demonstrated to shift through time most likely due to climate in pre-industrial times and human influence within the catchment and on regional dust emissions in industrial times. A Bayesian model was used to quantify the uncertainty associated with the quality of the varve appearance, the indistinct and intermittent varves, technical issues, observer judgement and depositional events. The varve chronology was integrated with an independent radiometric (^{14}C , ^{210}Pb , and ^{137}Cs) age-depth model to estimate the probabilities of over- and under-counting for different varve quality codes, reduce cumulative uncertainty, and correct for systematic under-counting.



725

This approach to building a varve chronology goes beyond the estimation of age uncertainty as it also constrains the uncertainty around varve thickness and thus sedimentation rates. The integration produced estimates of sedimentation rate that combine short-term as well as some long-term information, native to the varve and the radiometric chronologies. Furthermore, the approach offers an ensemble of plausible sedimentation rates from which flux and its uncertainty can be

730

calculated. This work not only establishes the chronology and sedimentation rates of Columbine Lake sediment to anchor future research at the site, it also demonstrates the potential for expanding high resolution reconstructions even to sites with indistinct and intermittent varves.



7 Appendix A

735 **Table A1. Difference in counts between marker layers between cores for each observer. Note that marker layers do not cross-coordinate between observers, only between cores for each observer. Difference is calculated as COL172-COL17-3.**

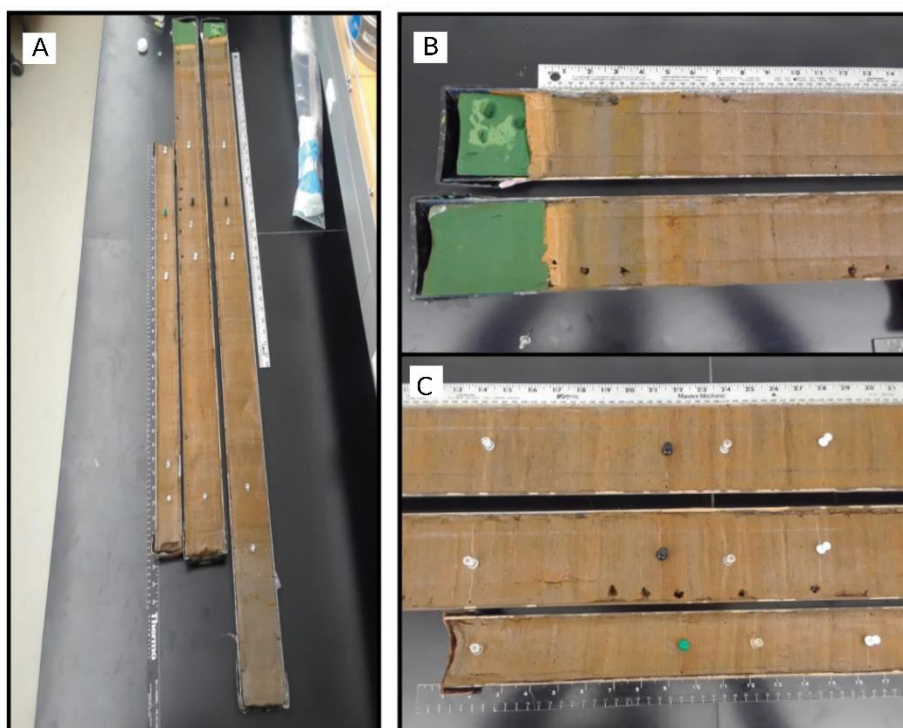
Marker Layer	COL172	COL173	Observer	Difference (years)	Difference (%)
1	699	660	1	39	5.7
2	275	308	1	-33	-11.3
3	951	1230	1	-279	-25.6
4	439	321	1	118	31.1
5	9	8	2	1	11.8
6	124	74	2	50	50.5
7	214	187	2	27	13.5
8	41	91	2	-50	-75.8
9	203	165	2	38	20.7
10	442	411	2	31	7.3
11	180	271	2	-91	-40.4
12	69	182	2	-113	-90.0
13	206	221	2	-15	-7.0
14	252	192	2	60	27.0
15	128	145	2	-17	-12.5
16	9	7	3	2	25.0
17	34	25	3	9	30.5
18	46	30	3	16	42.1
19	56	21	3	35	90.9
20	212	177	3	35	18.0
21	43	99	3	-56	-78.9
22	185	169	3	16	9.0
23	240	256	3	-16	-6.5
24	148	115	3	33	25.1
25	59	70	3	-11	-17.1
26	183	266	3	-83	-37.0
27	70	242	3	-172	-110.3
28	80	156	3	-76	-64.4
29	106	155	3	-49	-37.5
30	212	193	3	19	9.4
31	176	139	3	37	23.5



740 **Table A2. Observer- and core-specific varve sequence statistics of thickness and counts. Varve quality codes 4, 5, and 6 are excluded from the analysis except to calculate the cumulative length of indistinct sections. All units are millimetres unless otherwise noted.**

Core name	COL17-2			COL17-3		
	Obs 1	Obs 2	Obs 3	Obs 1	Obs 2	Obs 3
Minimum thickness	0.05	0.01	0.07	0.03	0.02	0.1
Maximum thickness	2.32	3.64	2.46	4.94	1.69	6.86
Median thickness	0.39	0.48	0.41	0.44	0.51	0.46
Mean thickness	0.43	0.56	0.48	0.48	0.56	0.51
SD thickness	0.23	0.35	0.26	0.24	0.25	0.37
Total indistinct section length	40	10	108	167	57	112

745



750 **Fig. A1. Tie points from three Columbine Lake cores. (A) shows COL-17-2 shown on the far right, COL-17-3 in the middle, and COL-16-1 on the left. The top of cores COL-17-3 and COL-17-2 are shown in (B). (C) is a section of the middle of all three cores with matching laminations marked with pins. Image credit: Wiman, C. (2019). Late Holocene hydroclimate and productivity in varved sediment at Columbine Lake, Colorado (Master thesis, Northern Arizona University).**

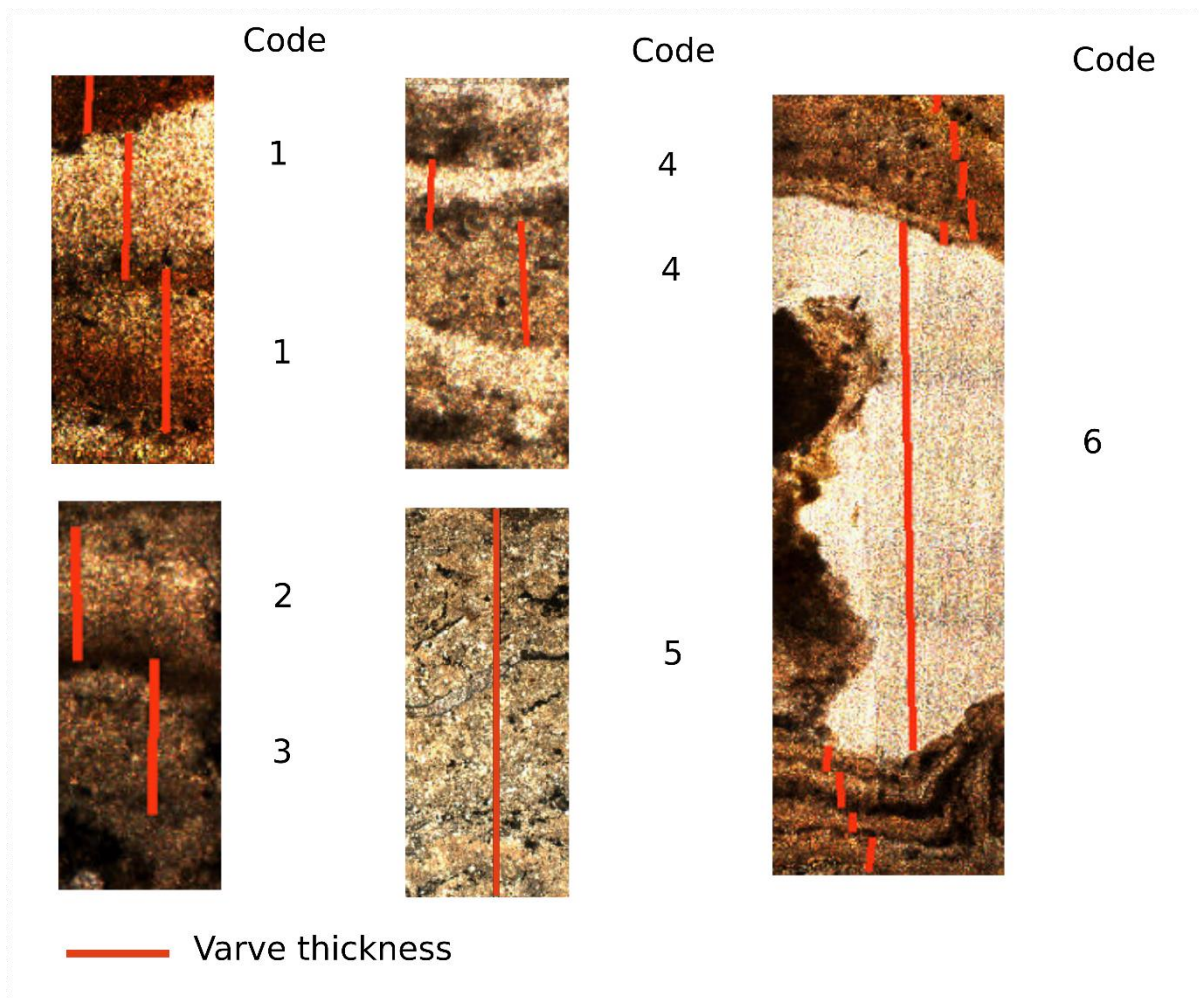
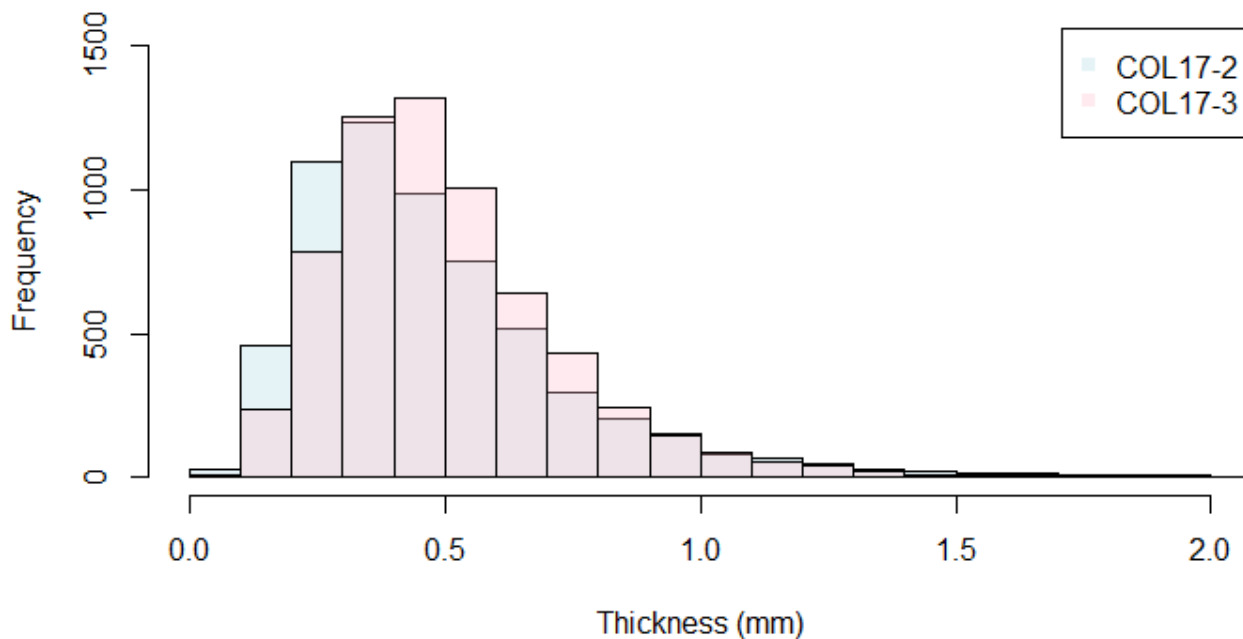


Fig. A2. Examples of varves appearance for each varve code.



755

Fig. A3. Comparison of varve thicknesses from varved sections (codes 1, 2, and 3) between COL17-2 and COL17-3.

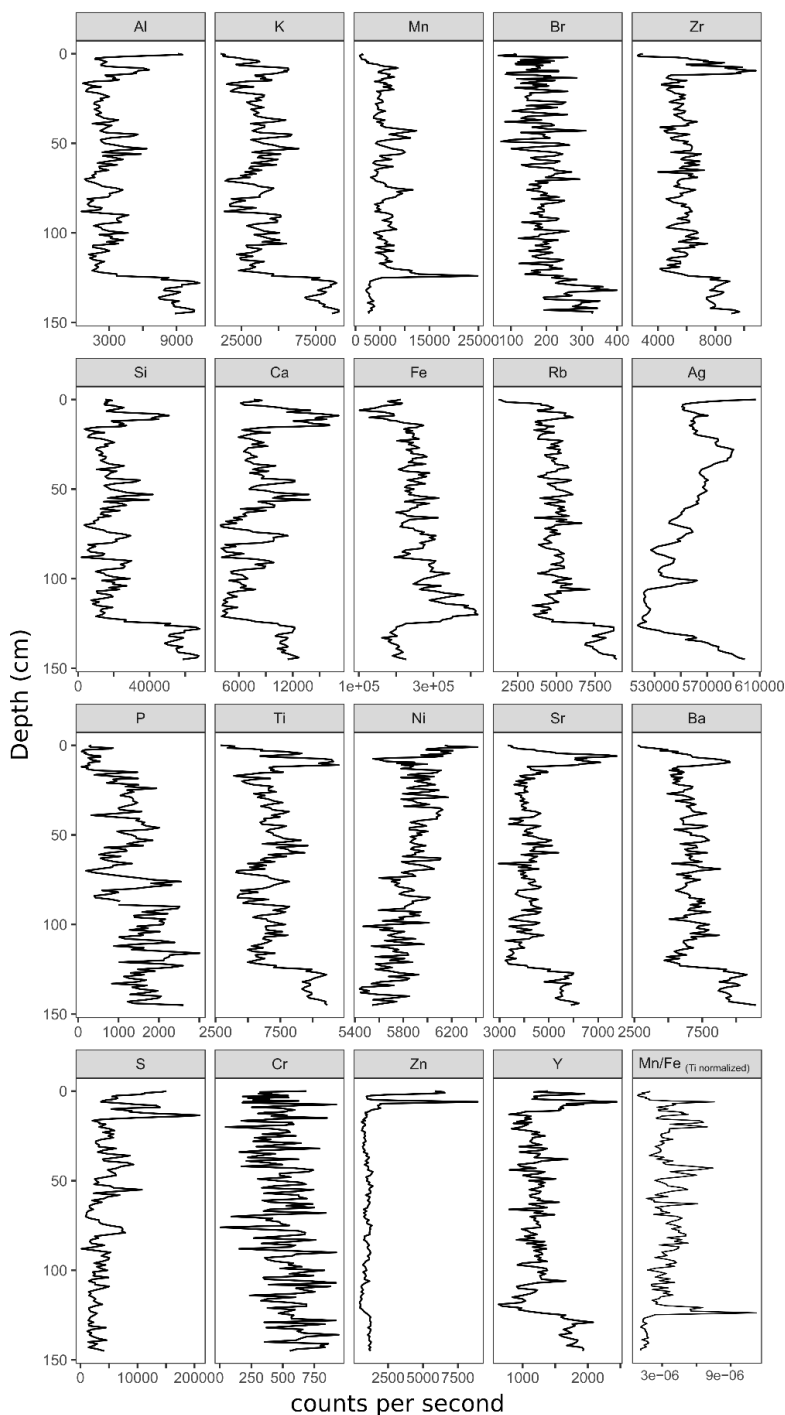
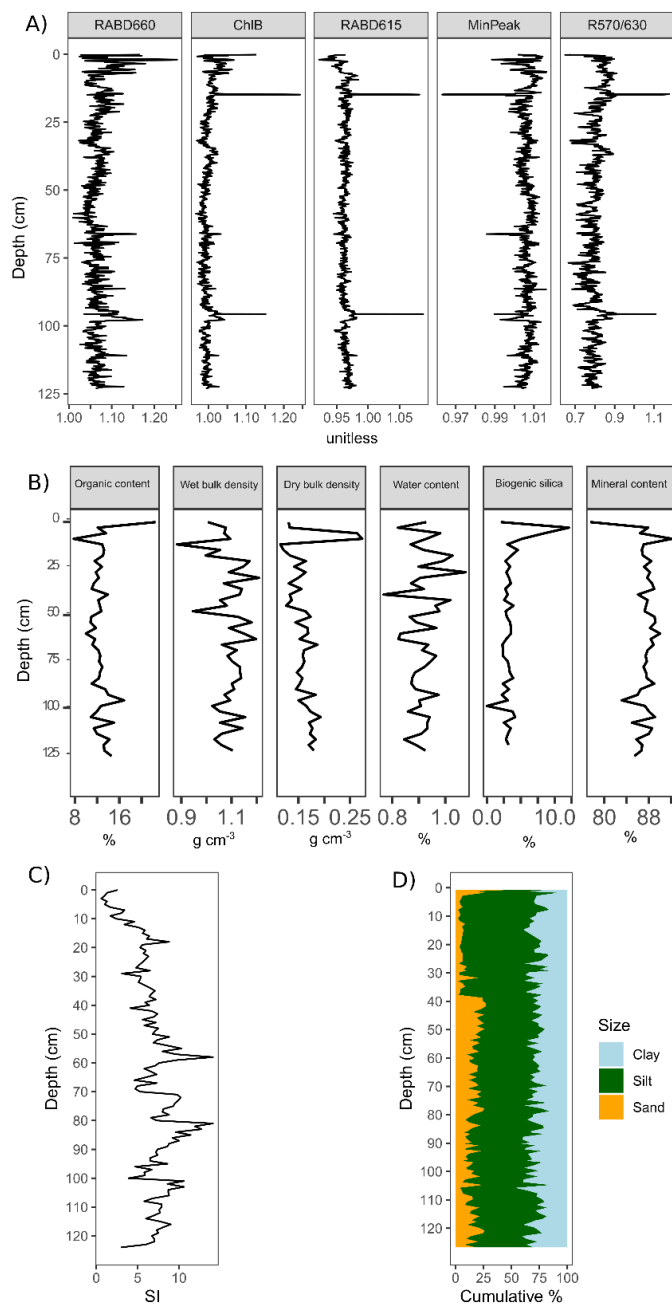
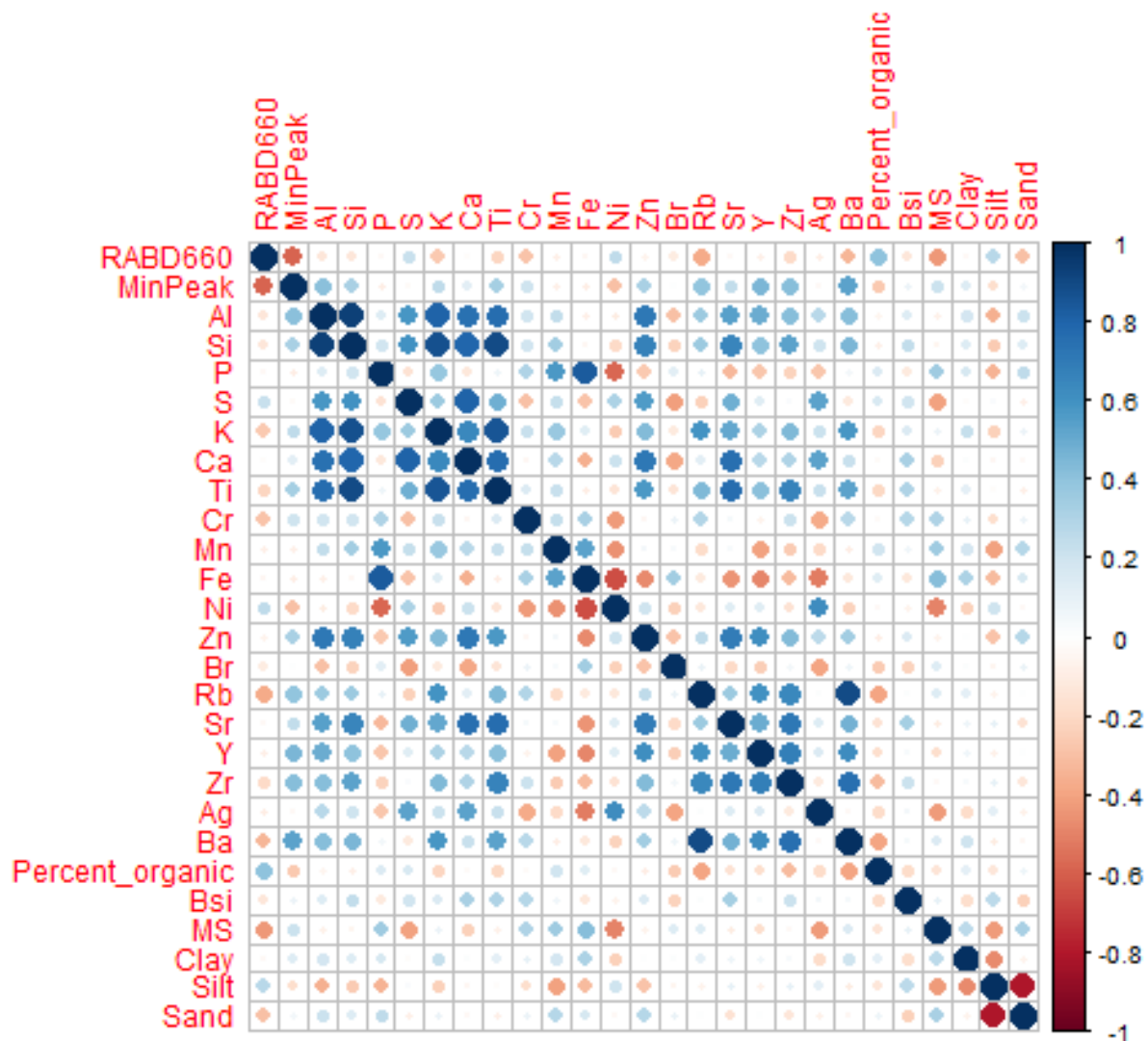


Fig. A4. X-Ray Fluorescence (XRF) elements measured on core COL17-3. Ratio Mn/Fe is normalized to Ti counts.



760

Fig. A5. Proxy dataset measured on core COL17-3 and used for the statistical analysis. (A) Ratios RABD660, RABD615 and ChIB are indicators of productivity. Ratios minPeak and R570/630 are indicators of clay minerals. (C) Destructive analyses including LOI (organic, water and mineral content), biogenic silica and wet and dry bulk density. (C) Magnetic susceptibility. (D) Grain size.



765

Fig. A6. Spearman's Rank correlation plot.

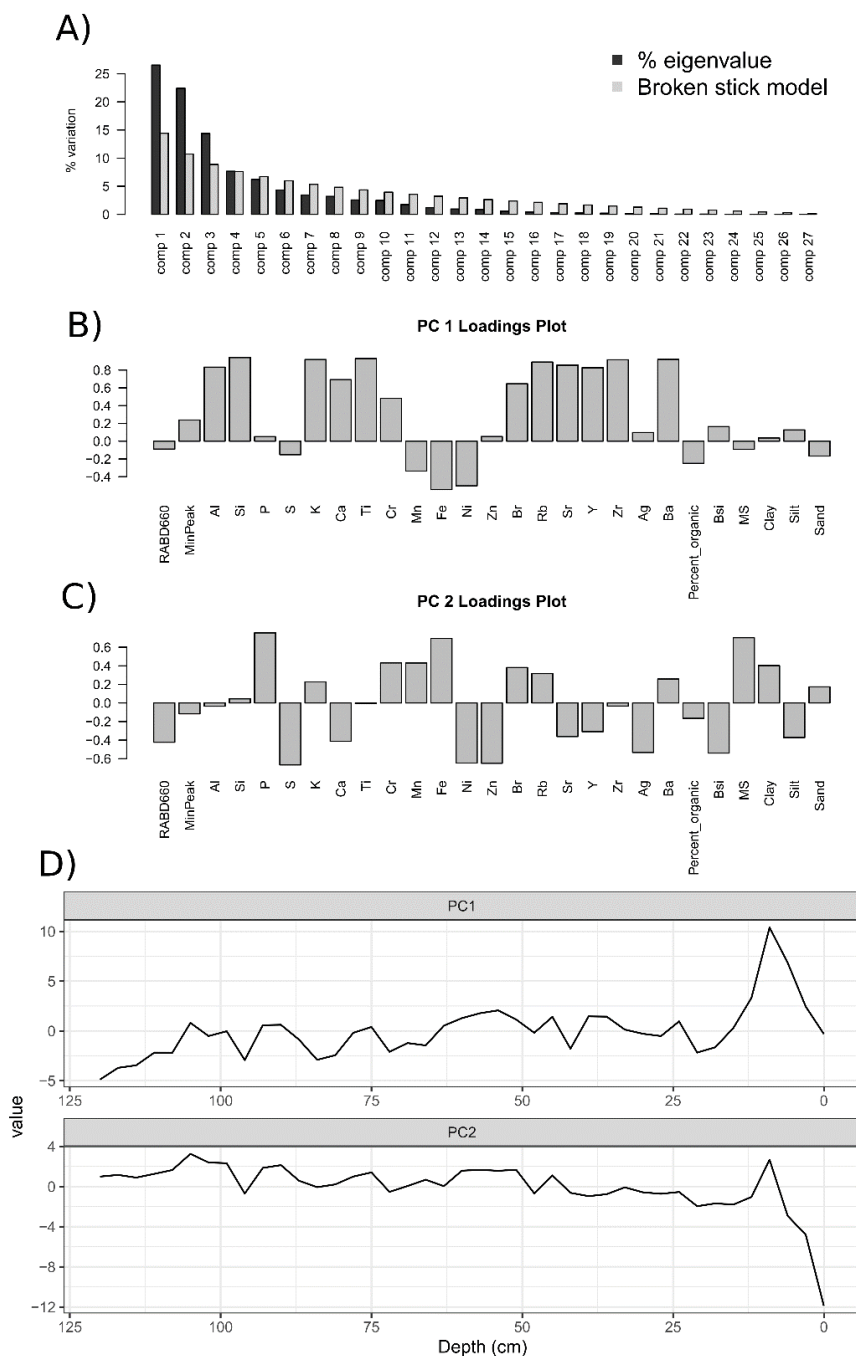


Fig. A7. (A) Broken stick model used to identify the significant principal components. Although three components are significant and explain 63.3 % of the variability, only components 1 and 2 are discussed in the manuscript. (B-C)

770 **Loadings and (D) scores for components 1 and 2.**

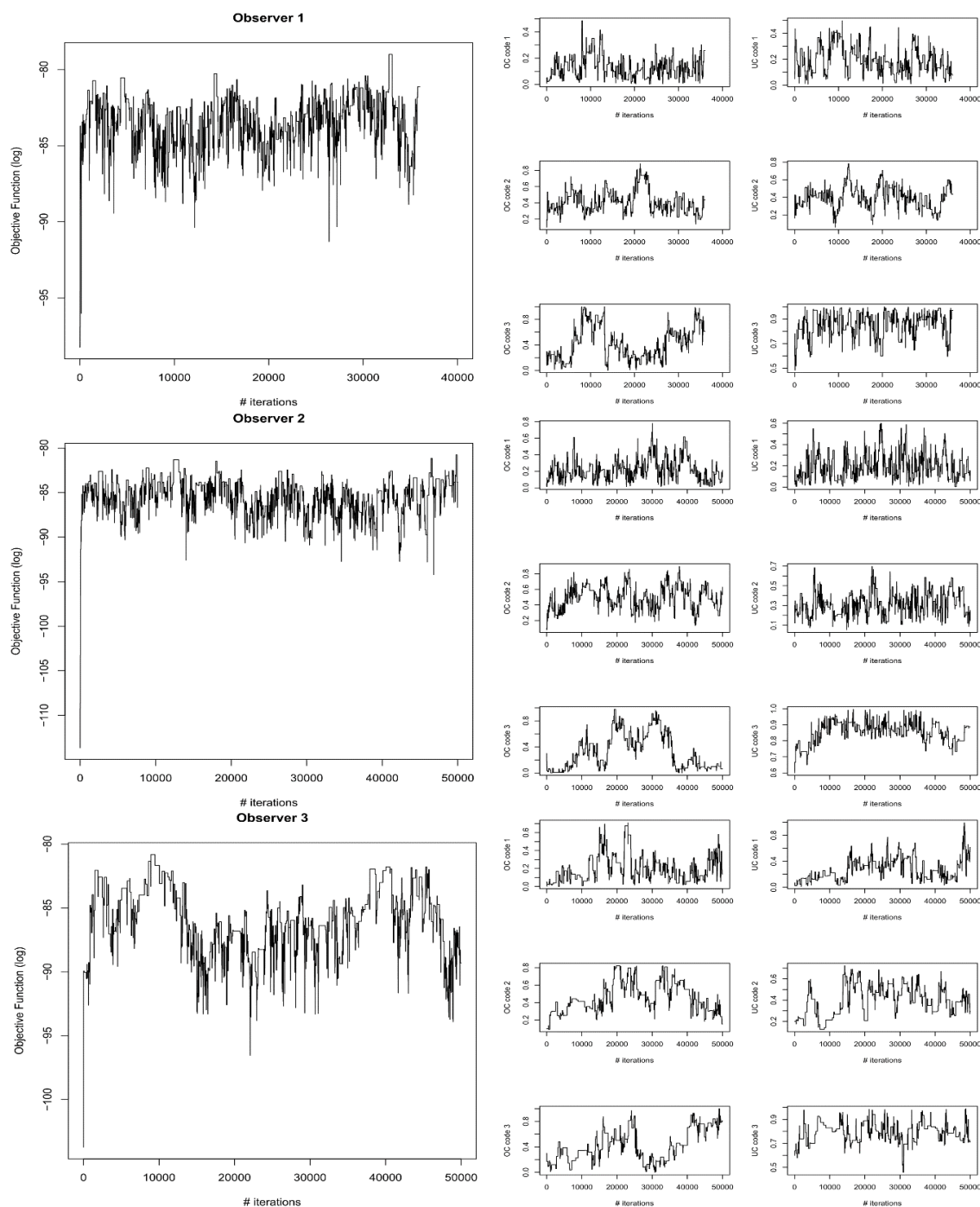


Fig. A8. Integrated model diagnostics. Objective function output value (left) and counting probabilities (right) for each iteration for observers 1 (top), 2 (middle), 3 (bottom). OC = over-counting. UC = under-counting. Number that follows OC/UC indicates the varve quality code.

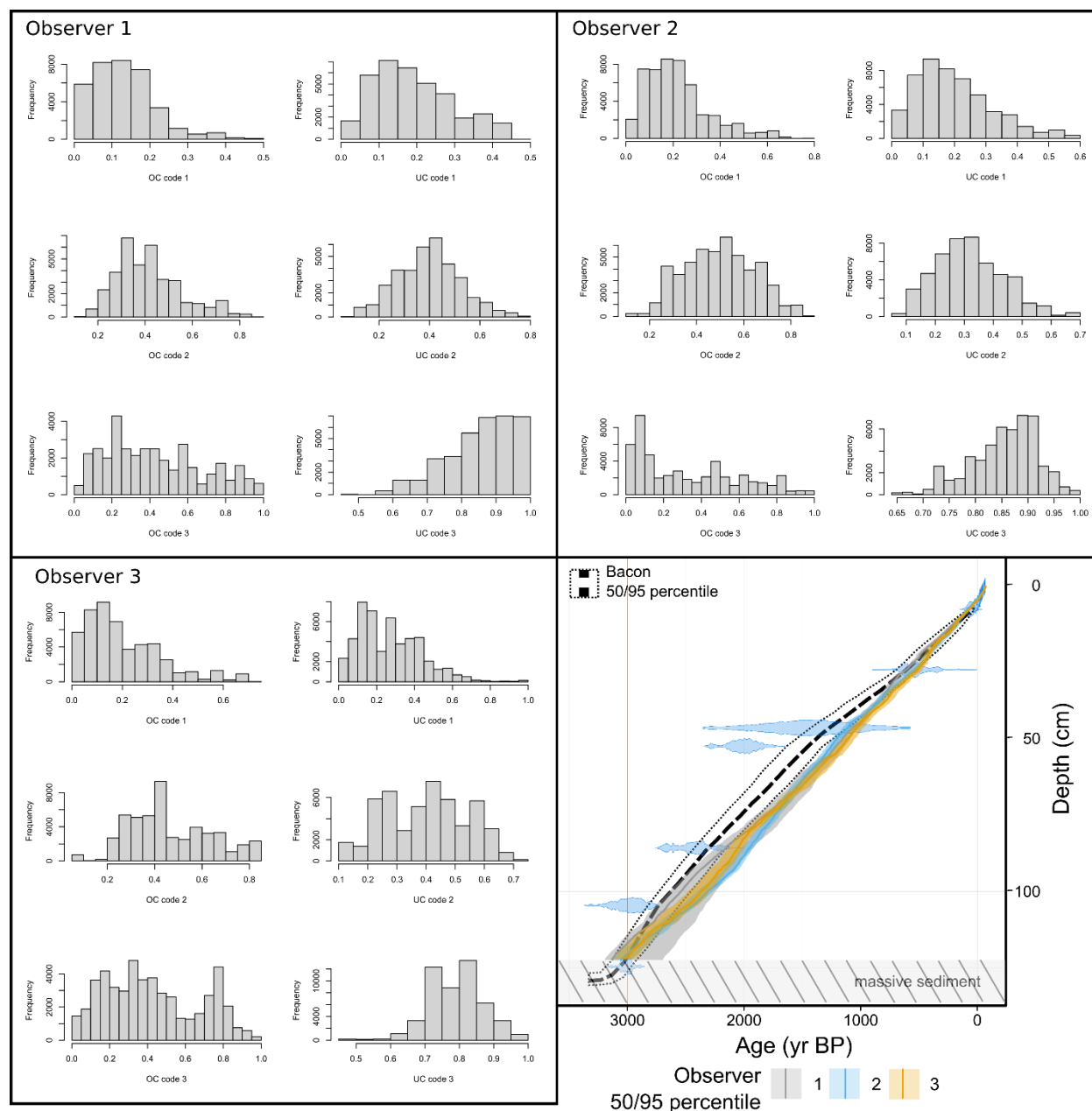


Fig. A9. Posterior probabilities of over- and under-counting for each observer for core COL17-3. Comparison between independent and integrated age-depth model. OC: over-counting. UC: under-counting. Code 1-3 indicate the varve quality codes 1, 2, 3.

780

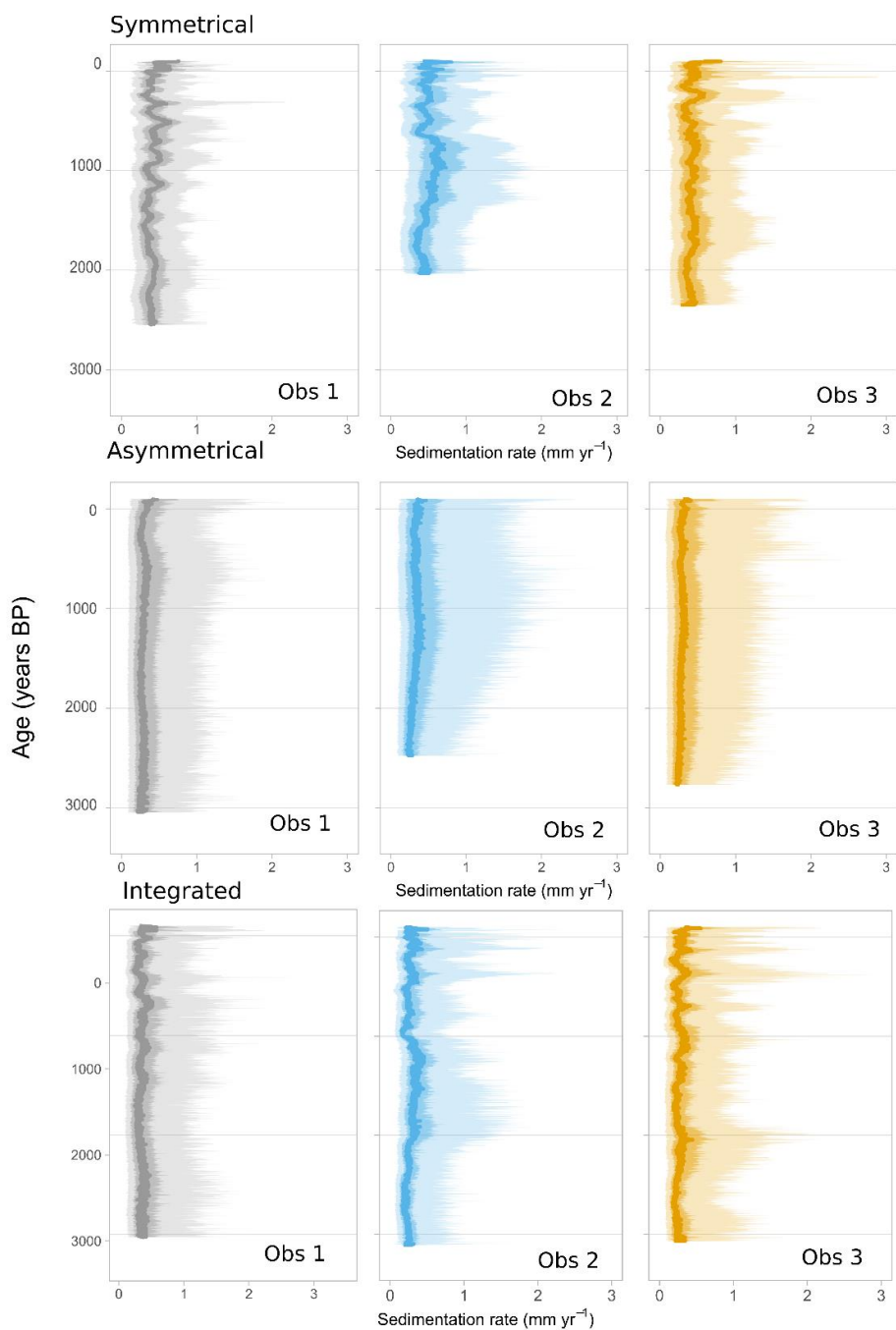
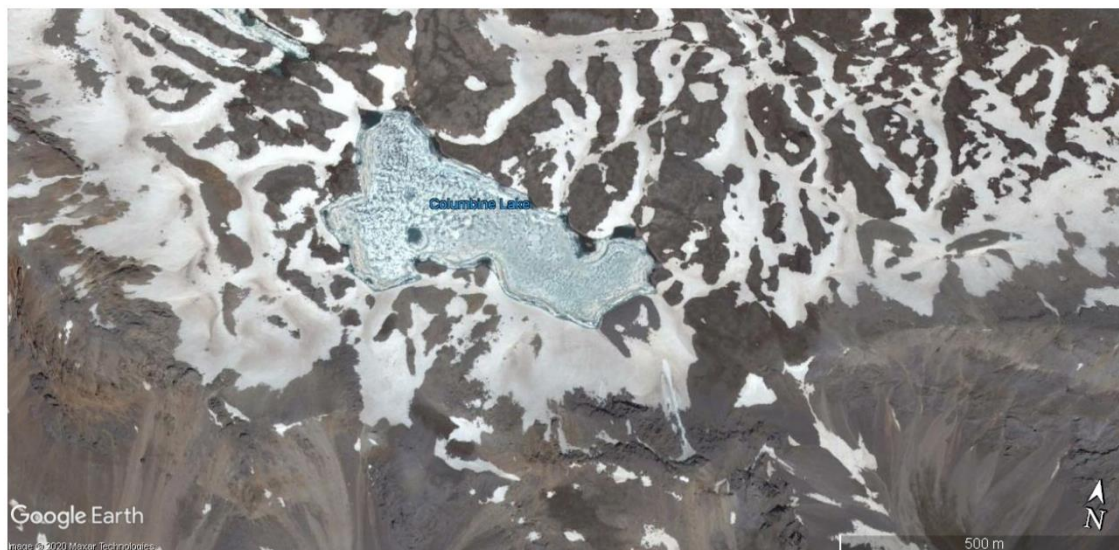


Fig. A10. Sedimentation rates for each observer for symmetrical varveR, asymmetrical varveR and the integrated models.



A) June 2012



B) June 2014



785 Fig. A11. Dust deposition in Columbine Lake catchment and frozen surface is frequently visible as a light brown tint on the snow. Image from (a) June 2012, and (b) June 2014. Map data: © Google Earth.

8 Code and data availability



Code for the original VarveR model can be found at [10.5281/zenodo.4733326](https://zenodo.org/record/4733326). Code for the varve and radiometric model integration can be found at [10.5281/zenodo.4744872](https://zenodo.org/record/4744872). Datasets containing radiometric measurements from Columbine Lake can be found at <https://doi.org/10.25384/SAGE.9879209.v1>. Datasets of varve delineations can be found at [10.6084/m9.figshare.14251400](https://doi.org/10.6084/m9.figshare.14251400). Datasets necessary to run the code (LiPD file and Bacon output file) can be found at [10.6084/m9.figshare.14417999](https://doi.org/10.6084/m9.figshare.14417999). Dataset containing proxy measurements produced in this study can be found at [10.6084/m9.figshare.14265644](https://doi.org/10.6084/m9.figshare.14265644) for the review process and will be uploaded to NOAA World Data Service for Paleoclimatology upon publication.

795 **9 Author contribution**

SHA and NPM conceptualized the study. CW sampled and embedded the sediments, SHA, CW, and SP measured varves, and SEM measured lead samples. MAL ran the Plum-Bacon model. SHA and NPM created and modified the Bayesian models, and SHA ran the models. SHA visualized the data and drafted the original manuscript. All authors contributed to the review and editing.

800 **10 Competing interests**

The authors declare that they have no conflict of interest.

11 Acknowledgments

This research was funded by Bob and Judi Braudy and we are grateful for their support. MAL was partially funded by CONACYT CB-2016-01-284451 and COVID19 312772 grants and a RDCOMM grant. We thank D Buscombe for letting us use the bathymetric equipment, RS Anderson for the identification of macrofossils for ^{14}C dating, K Whitacre for lab assistance, Rosalind Wu from the San Juan National Forest Service for working with us to obtain permits for sampling Columbine Lake, C Routson and D Kaufman for helpful feedback on the manuscript, Quality Thin Sections for producing the thin sections, and C Ebert for conducting ^{14}C dating at IonPlus in Zurich. We thank E Yackulic, C Mogen, W Wiman, C Routson, A Wong, A Platt, J Chaffeur, E Broadman, and M Caron for the help in the field.

810 **12 References**

Anderson, B. R. Y., Dean, W. E., Bradbury, P. and Love, D.: Meromictic Lakes and Varved Sediments, 19 [online] Available from: <https://pubs.usgs.gov/bul/1607/report.pdf>, 1985.



- Anderson, R. S., Smith, S. J., Lynch, A. M. and Geils, B. W.: The pollen record of a 20th century spruce beetle (*Dendroctonus rufipennis*) outbreak in a Colorado subalpine forest, USA, *For. Ecol. Manage.*, 260(4), 448–455, 815 doi:10.1016/j.foreco.2010.05.001, 2010.
- Appleby, P.: Chronostratigraphic techniques in recent sediments, in *Tracking Environmental Change Using Lake Sediments. Volume 1*, edited by W. Last and J. P. Smol, pp. 171–203, Kluwer Academic Publishers, Dordrecht., 2001.
- Appleby, P. G. and Oldfield, F.: The calculation of lead-210 dates assuming a constant rate of supply of unsupported ²¹⁰Pb to the sediment, *CATENA*, 5(1), 1–8, doi:10.1016/S0341-8162(78)80002-2, 1978.
- 820 Aquino-López, M. A., Blaauw, M., Christen, J. A. and Sanderson, N. K.: Bayesian Analysis of ²¹⁰Pb Dating, *J. Agric. Biol. Environ. Stat.*, 23, 317–333, doi:10.1007/s13253-018-0328-7, 2018.
- Arcusa, S. H., McKay, N. P., Routson, C. C. and Munoz, S. E.: Dust-drought interactions over the last 15,000 years: A network of lake sediment records from the San Juan Mountains, Colorado, *The Holocene*, doi:10.1177/0959683619875192, 2019.
- 825 Arcusa, S. H., Schneider, T., Mosquera, P. V., Vogel, H., Kaufman, D. S., Szidat, S. and Grosjean, M.: Late Holocene tephrostratigraphy from Cajas National Park, southern Ecuador, *Andean Geol.*, 47(3), 508–528, doi:http://dx.doi.org/10.5027/andgeoV47n3-3301, 2020.
- Baker, W. L.: Variable forest structure and fire reconstructed across historical ponderosa pine and mixed conifer landscapes of the San Juan Mountains, Colorado, *Land*, 9(1), 1–35, doi:10.3390/land9010003, 2020.
- 830 Blaauw, M. and Christen, J. A.: Flexible paleoclimate age-depth models using an autoregressive gamma process, *Bayesian Anal.*, 6(3), 457–474, doi:10.1214/11-BA618, 2011.
- Blair, R. and Bracksieck, G.: *The Eastern San Juan Mountains.*, edited by R. Blair and G. Bracksieck, University Press of Colorado., 2011.
- Blockley, S. P. E., Ramsey, C. B., Lane, C. S. and Lotter, A. F.: Improved age modelling approaches as exemplified by the 835 revised chronology for the Central European varved lake Soppensee, *Quat. Sci. Rev.*, 27(1–2), 61–71, doi:10.1016/j.quascirev.2007.01.018, 2008.
- Boers, N., Goswami, B. and Ghil, M.: A complete representation of uncertainties in layer-counted paleoclimatic archives, *Clim. Past*, 13(9), 1169–1190, doi:10.5194/cp-13-1169-2017, 2017.
- Bonk, A., Tylmann, W., Goslar, T., Wacnik, A. and Grosjean, M.: Comparing varve counting and ¹⁴C-AMS chronologies in 840 the sediments of lake Żabińskie, Northeastern Poland: Implications for accurate ¹⁴C dating of lake sediments, *Geochronometria*, 42, 159–171, 2015.
- Brauer, A., Hajdas, I., Blockley, S. P. E., Bronk Ramsey, C., Christl, M., Ivy-Ochs, S., Moseley, G. E., Nowaczyk, N. N., Rasmussen, S. O., Roberts, H. M., Spötl, C., Staff, R. A. and Svensson, A.: The importance of independent chronology in integrating records of past climate change for the 60-8ka INTIMATE time interval, *Quat. Sci. Rev.*, 106, 47–66, 845 doi:10.1016/j.quascirev.2014.07.006, 2014.



- Bronk Ramsey, C.: Radiocarbon calibration and analysis of stratigraphy: the OxCal program, *Radiocarbon*, 37(2), 425–430, 1995.
- Bruel, R. and Sabatier, P.: serac: a R package for ShortlivEd RADionuclide Chronology of recent sediment cores, 1–38, doi:10.31223/osf.io/f4yma, 2020.
- 850 Buck, C. E., Higham, T. F. G. and Lowe, D. J.: Bayesian tools for tephrochronology, *The Holocene*, 13(5), 639–647, doi:10.1191/0959683603hl652ft, 2003.
- Butz, C., Grosjean, M., Poraj-Górska, A., Enters, D., Tylmann, W. and Butz, C.: Sedimentary Bacteriopheophytin a as an indicator of meromixis in varved lake sediments of Lake Jaczno , north-east Poland , AD 1891 – 2010, *Glob. Planet. Change*, 144, 1–26, doi:10.1016/j.gloplacha.2016.07.012, 2016.
- 855 Butz, C., Grosjean, M., Goslar, T. and Tylmann, W.: Hyperspectral imaging of sedimentary bacterial pigments: a 1700-year history of meromixis from varved Lake Jaczno, northeast Poland, *J. Paleolimnol.*, 58(1), 57–72, doi:10.1007/s10933-017-9955-1, 2017.
- Carrara, P.: Deglaciation and postglacial treeline fluctuation in the northern San Juan Mountains, Colorado, U.S. Geol. Soc. Prof. Pap. 1782, 1–48 [online] Available from: <http://pubs.usgs.gov/pp/1782/>, 2011.
- 860 Conway, H., Gades, A. and Raymond, C. F.: Albedo of dirty snow during conditions of melt, *Water Resour. Res.*, 32(6), 1713–1718, 1996.
- Cuven, S., Francus, P. and Lamoureux, S. F.: Estimation of grain size variability with micro X-ray fluorescence in laminated lacustrine sediments, Cape Bounty, Canadian High Arctic, *J. Paleolimnol.*, 44(3), 803–817, doi:10.1007/s10933-010-9453-1, 2010.
- 865 Dean, W. J.: Determination of carbonate and organic matter in calcareous sediments and sedimentary rocks by loss on ignition: comparison with other methods, *J. Sediment. Petrol.*, 44(I), 242–248, doi:10.1128/JCM.01030-15, 1974.
- Desloges, J. R.: Varve deposition and the sediment yield record at three small lakes of the southern Canadian Cordillera, *Arct. Alp. Res.*, 26(2), 130–140, doi:10.2307/1551776, 1994.
- Dräger, N., Theuerkauf, M., Szeroczyńska, K., Wulf, S., Tjallingii, R., Plessen, B., Kienel, U. and Brauer, A.: Varve
870 microfacies and varve preservation record of climate change and human impact for the last 6000 years at Lake Tiefer See (NE Germany), *The Holocene*, 27(3), 450–464, doi:10.1177/0959683616660173, 2017.
- Fortin, D., Praet, N., McKay, N. P., Kaufman, D. S., Jensen, B. J. L., Haeussler, P. J., Buchanan, C. and De Batist, M.: New approach to assessing age uncertainties – The 2300-year varve chronology from Eklutna Lake, Alaska (USA), *Quat. Sci. Rev.*, 203, 90–101, doi:10.1016/j.quascirev.2018.10.018, 2019.
- 875 Francus, P., Bradley, R. S., Lewis, T., Abbott, M., Retelle, M. and Stoner, J. S.: Limnological and sedimentary processes at Sawtooth Lake, Canadian High Arctic, and their influence on varve formation, *J. Paleolimnol.*, 40(3), 963–985, doi:10.1007/s10933-008-9210-x, 2008.
- Geyh, M., Schotterer, U. and Grosjean, M.: Temporal changes of the ¹⁴C reservoir effect in lakes, *Radiocarbon*, 40(2), 921–931, 1998.



- 880 Geyh, M. A., Grosjean, M., Núñez, L. and Schotterer, U.: Radiocarbon reservoir effect and the timing of the late-glacial/early Holocene humid phase in the Atacama Desert (Northern Chile), *Quat. Res.*, 52(2), 143–153, doi:10.1006/qres.1999.2060, 1999.
- Gilli, A., Anselmetti, F. S., Glur, L. and Wirth, S. B.: Lake Sediments as Archives of Recurrence Rates and Intensities of Past Flood Events, in *Dating Torrential Processes on Fans and Cones*, edited by M. Schneuwly-Bollschweiler, pp. 225–242, 885 Springer Science+Business Media, Dordrecht., 2013.
- Guyard, H., Chapron, E., St-Onge, G., Anselmetti, F. S., Arnaud, F., Magand, O., Francus, P. and Res, M.-A.: High-altitude varve records of abrupt environmental changes and mining activity over the last 4000 years in the Western French Alps (Lake Bramant, Grandes Rousses Massif), *Quat. Sci. Rev.*, 26, 2644–2660, doi:10.1016/j.quascirev.2007.07.007, 2007.
- Helama, S., Jones, P. D. and Briffa, K. R.: Dark Ages Cold Period: A literature review and directions for future research, 890 *Holocene*, 27(10), 1600–1606, doi:10.1177/0959683617693898, 2017.
- Hughen, K. A., Southon, J. R., Bertrand, C. J. H., Frantz, B. and Zerbeño, P.: Cariaco basin calibration update: Revisions to calendar and ¹⁴C chronologies for core PL07-58PC, *Radiocarbon*, 46(3), 1161–1187, doi:10.1017/S0033822200033075, 2004.
- Juggins, S.: rioja: Analysis of Quaternary Science Data, [online] Available from: <https://cran.r-project.org/package=rioja>, 895 2020.
- Kneller, B.: Beyond the turbidite paradigm: Physical models for deposition of turbidites and their implications for reservoir prediction, *Geol. Soc. Spec. Publ.*, 94(December), 31–49, doi:10.1144/GSL.SP.1995.094.01.04, 1995.
- Krishnaswamy, S., Lal, D., Martin, J. M. and Meybeck, M.: Geochronology of lake sediments, *Earth Planet. Sci. Lett.*, 11(1–5), 407–414, doi:10.1016/0012-821X(71)90202-0, 1971.
- 900 Lamb, M. P. and Mohrig, D.: Do hyperpycnal-flow deposits record river-flood dynamics? *Geology*, 37(12), 1067–1070, doi:10.1130/G30286A.1, 2009.
- Lamoureux, S. F.: Embedding unfrozen lake sediments for thin section preparation, *J. Paleolimnol.*, 10(2), 141–146, 1994.
- Lamoureux, S.F.: Varve chronology techniques. In: Last, W.M., Smol, J.P. (Eds.), *Developments in Paleoenvironmental Research (DPER), Tracking Environmental Change Using Lake Sediments: Basin Analysis, Coring, and Chronological* 905 *Techniques*, vol. 1. Kluwer, Dordrecht, pp. 247e260. http://dx.doi.org/10.1007/0-306-47669-X_11, 2001.
- Le, S., Josse, J. and Husson, F.: FactoMineR: An R package for multivariate analysis, *J. Stat. Softw.*, 25(1), 1–18, 2008.
- Lewis, T., Francus, P., Bradley, R. S. and Kanamaru, K.: An automated system for the statistical analysis of sediment texture and structure at the micro scale, *Comput. Geosci.*, 36(10), 1374–1383, doi:10.1016/j.cageo.2010.03.018, 2010.
- Li, J., Okin, G. S., McKenzie Skiles, S. and Painter, T. H.: Relating variation of dust on snow to bare soil dynamics in the 910 western United States, *Environ. Res. Lett.*, 8(4), doi:10.1088/1748-9326/8/4/044054, 2013.
- Lipman, P. W. and McIntosh, W. C.: Tertiary Volcanism in the Eastern San Juan Mountains, in *The Eastern San Juan Mountains: Their Geology, Ecology, Human History*, edited by R. Blair and G. Bracksieck, University Press of Colorado., 2011.



- Makri, S., Rey, F., Gobet, E., Gilli, A., Tinner, W. and Grosjean, M.: Early human impact in a 15,000-year high-resolution
915 hyperspectral imaging record of paleoproduction and anoxia from a varved lake in Switzerland, *Quat. Sci. Rev.*, 239,
106335, doi:10.1016/j.quascirev.2020.106335, 2020.
- Mckay, N., Emile-Geay, J. and Khider, D.: GeoChronR – an R package to model, analyze, and visualize age-uncertain data,
Geochronology, 3, 149-169, <https://doi.org/10.5194/gchron-3-149-2021>, 2021.
- McKay, N. P.: Development package for varve counting, modeling and analysis., 2019.
- 920 Mortlock, R. A. and Froelich, P. N.: A simple method for the rapid determination of biogenic opal in pelagic marine
sediments, *Deep Sea Res. Part A, Oceanogr. Res. Pap.*, 36(9), 1415–1426, doi:10.1016/0198-0149(89)90092-7, 1989.
- Mulder, T. and Syvitski, J. P. M.: Turbidity currents generated at river mouths during exceptional discharges to the world
oceans, *J. Geol.*, 103(3), 285–299, doi:10.1086/629747, 1995.
- Mulder, T., Migeon, S., Savoye, B. and Faugeres, J.-C.: Inversely graded turbidite sequences in the deep Mediterranean: A
925 record of deposits from flood-generated turbidity currents? *Geo-Marine Lett.*, 21(2), 86–93, doi:10.1007/s003670100071,
2001.
- Naeher, S., Gilli, A., North, R. P., Hamann, Y. and Schubert, C. J.: Tracing bottom water oxygenation with sedimentary
Mn/Fe ratios in Lake Zurich, Switzerland, *Chem. Geol.*, 352, 125–133, doi:10.1016/j.chemgeo.2013.06.006, 2013.
- Neff, J. C., Ballantyne, A. P., Farmer, G. L., Mahowald, N. M., Conroy, J. L., Landry, C. C., Overpeck, J. T., Painter, T. H.,
930 Lawrence, C. R. and Reynolds, R. L.: Increasing eolian dust deposition in the western United States linked to human
activity, *Nat. Geosci.*, 1(3), 189–195, doi:10.1038/ngeo133, 2008.
- O’Sullivan, P. E.: Annually-laminated lake sediments and the study of Quaternary environmental changes - a review, *Quat.
Sci. Rev.*, 1(4), 245–313, doi:10.1016/0277-3791(83)90008-2, 1983.
- Ojala, A. E. K. and Tiljander, M.: Testing the fidelity of sediment chronology: Comparison of varve and paleomagnetic
935 results from Holocene lake sediments from central Finland, *Quat. Sci. Rev.*, 22(15–17), 1787–1803, doi:10.1016/S0277-
3791(03)00140-9, 2003.
- Ojala, A. E. K., Saarinen, T. and Salonen, V. P.: Preconditions for the formation of annually laminated lake sediments in
southern and central Finland, *Boreal Environ. Res.*, 5(3), 243–255, 2000.
- Ojala, A. E. K., Francus, P., Zolitschka, B., Besonen, M. and Lamoureux, S. F.: Characteristics of sedimentary varve
940 chronologies - A review, *Quat. Sci. Rev.*, 43, 45–60, doi:10.1016/j.quascirev.2012.04.006, 2012.
- Palmer, A. P., Bendle, J. M., MacLeod, A., Rose, J. and Thorndycraft, V. R.: The micromorphology of glaciolacustrine
varve sediments and their use for reconstructing palaeoglaciological and palaeoenvironmental change, *Quat. Sci. Rev.*, 226,
105964, doi:10.1016/j.quascirev.2019.105964, 2019.
- Parnell, A. C., Buck, C. E. and Doan, T. K.: A review of statistical chronology models for high-resolution, proxy-based
945 Holocene palaeoenvironmental reconstruction, *Quat. Sci. Rev.*, 30(21–22), 2948–2960, doi:10.1016/j.quascirev.2011.07.024,
2011.



- Preibisch, S., Saalfeld, S. and Tomancak, P.: Globally optimal stitching of tiled 3D microscopic image acquisitions, *Bioinformatics*, 25(11), 1463–1465, doi:10.1093/bioinformatics/btp184, 2009.
- R Core Team: R: A Language and Environment for Statistical Computing, [online] Available from: <https://www.r-project.org/>, 2019.
- 950 Rein, B. and Sirocko, F.: In-situ reflectance spectroscopy – analysing techniques for high-resolution pigment logging in sediment cores, *Int. J. Earth Sci.*, 91, 950–954, 2002.
- Rodysill, J. R., Anderson, L., Cronin, T. M., Jones, M. C., Thompson, R. S., Wahl, D. B., Willard, D. A., Addison, J. A., Alder, J. R., Anderson, K. H., Anderson, L., Barron, J. A., Bernhardt, C. E., Hostetler, S. W., Kehrwald, N. M., Khan, N. S.,
- 955 Richey, J. N., Starratt, S. W., Strickland, L. E., Toomey, M. R., Treat, C. C. and Wingard, G. L.: A North American Hydroclimate Synthesis (NAHS) of the Common Era, *Glob. Planet. Change*, 162(December 2017), 175–198, doi:10.1016/j.gloplacha.2017.12.025, 2018.
- Routson, C. C., Woodhouse, C. A. and Overpeck, J. T.: Second century megadrought in the Rio Grande headwaters, Colorado: How unusual was medieval drought? *Geophys. Res. Lett.*, 38(22), 1–5, doi:10.1029/2011GL050015, 2011.
- 960 Routson, C. C., Overpeck, J. T., Woodhouse, C. A. and Kenney, W. F.: Three millennia of southwestern north American dustiness and future implications, *PLoS One*, 11(2), 1–20, doi:10.1371/journal.pone.0149573, 2016.
- Routson, C. C., Arcusa, S. H., McKay, N. P. and Overpeck, J. T.: A 4500-year-long record of southern Rocky Mountain dust deposition, *Geophys. Res. Lett.*, 46, 2019GL083255, doi:10.1029/2019GL083255, 2019.
- Schlolaut, G., Marshall, M. H., Brauer, A., Nakagawa, T., Lamb, H. F., Staff, R. A., Bronk Ramsey, C., Bryant, C. L.,
- 965 Brock, F., Kossler, A., Tarasov, P. E., Yokoyama, Y., Tada, R. and Haraguchi, T.: An automated method for varve interpolation and its application to the Late Glacial chronology from Lake Suigetsu, Japan, *Quat. Geochronol.*, 13, 52–69, doi:10.1016/j.quageo.2012.07.005, 2012.
- Schneider, T., Hampel, H., Mosquera, P. V., Tylmann, W. and Grosjean, M.: Paleo-ENSO revisited: Ecuadorian Lake Pallcacocha does not reveal a conclusive El Niño signal, *Glob. Planet. Change*, 168(June), 54–66,
- 970 doi:10.1016/j.gloplacha.2018.06.004, 2018.
- Sheppard, P. R., Comrie, A. C., Packin, G. D., Angersbach, K. and Hughes, M. K.: The climate of the US Southwest, *Clim. Res.*, 21, 219–238, 2002.
- Tian, J., Brown, T. A. and Hu, F. S.: Comparison of varve and ^{14}C chronologies from Steel Lake, Minnesota, USA, *The Holocene*, 15(4), 510–517, doi:10.1191/0959683605hl828rp, 2005.
- 975 Trachsel, M., Grosjean, M., Schnyder, D., Kamenik, C. and Rein, B.: Scanning reflectance spectroscopy (380–730 nm): A novel method for quantitative high-resolution climate reconstructions from minerogenic lake sediments, *J. Paleolimnol.*, 44(4), 979–994, doi:10.1007/s10933-010-9468-7, 2010.
- Western Regional Climate Center: Cooperative Climatological Data Summaries, [online] Available from: <https://wrcc.dri.edu/cgi-bin/cliMAIN.pl?co7656>, 2018.



- 980 Yackulic, E.: Productivity and temperature variability over the past 15000 years at a small alpine lake in the southern San Juan Mountains, Colorado, Northern Arizona University., 2017.
Zander, P. D., Szidat, S., Kaufman, D. S., Żarczyński, M., Poraj-górska, A. I. and Grosjean, M.: Miniature radiocarbon measurements ($< 150 \mu\text{g C}$) from sediments of Lake Żabińskie, Poland: effect of precision and dating density on age-depth models, *Geochronology*, (December), 63–79, 2019.
- 985 Żarczyński, M., Tylmann, W. and Goslar, T.: Multiple varve chronologies for the last 2000 years from the sediments of Lake Żabińskie (northeastern Poland) – Comparison of strategies for varve counting and uncertainty estimations, *Quat. Geochronol.*, 47(January), 107–119, doi:10.1016/j.quageo.2018.06.001, 2018.
Żarczyński, M., Szymańska, J. and Tylmann, W.: Grain-Size Distribution and Structural Characteristics of Varved Sediments from Lake Żabińskie (Northeastern Poland), *Quaternary*, 2(1), 8, doi:10.3390/quat2010008, 2019a.
- 990 Żarczyński, M., Wacnik, A. and Tylmann, W.: Tracing lake mixing and oxygenation regime using the Fe/Mn ratio in varved sediments: 2000 year-long record of human-induced changes from Lake Żabińskie (NE Poland), *Sci. Total Environ.*, 657, 585–596, doi:10.1016/j.scitotenv.2018.12.078, 2019b.
Zhai, Q., Guo, Z., Li, Y. and Li, R.: Annually laminated lake sediments and environmental changes in Bashang Plateau, North China, *Palaeogeogr. Palaeoclimatol. Palaeoecol.*, 241(1), 95–102, doi:10.1016/j.palaeo.2006.06.011, 2006.
- 995 Zimmerman, S. R. H. and Wahl, D. B.: Holocene paleoclimate change in the western US: The importance of chronology in discerning patterns and drivers, *Quat. Sci. Rev.*, 246, 106487, doi:10.1016/j.quascirev.2020.106487, 2020.
Zolitschka, B., Francus, P., Ojala, A. E. K. and Schimmelmann, A.: Varves in lake sediments - a review, *Quat. Sci. Rev.*, 117, 1–41, doi:10.1016/j.quascirev.2015.03.019, 2015.